Joint Biotechnology Master Program

Palestine Polytechnic University
Deanship of Graduate Studies and Scientific Research

Bethlehem University
Faculty of Science

Identification of a Missense Mutation in *LRP4* Gene in a Palestinian Family with Cenani-Lenz Syndactyly

By

Lama Abbas Juneidi

In Partial Fulfillment of the Requirements for the Degree

Master of Biotechnology

May, 2021

The undersigned hereby certify that they have read and recommend to the Faculty of Scientific Research and Higher Studies at the Palestine Polytechnic University and the Faculty of Science at Bethlehem University for acceptance a thesis entitled:

"Identification of a Missense Mutation in *LRP4* gene in a Palestinian Family with Cenani-Lenz Syndactyly"

by

Lama Abbas Juneidi

A thesis submitted in partial fulfillment of the requirements for the degree of Master of Science in biotechnology.

Graduate Advisory Committee:

Committee Member(Student's Supervisor)	Date
Dr. Hashem Shahin – Bethlehem University	
Committee Member (Internal Examiner)	Date
Dr. Ghassan Handal – Bethlehem University	
Committee Member (External Examiner)	Date
Dr. Zaidoun Salah – Al-Quds University	

Approved for the Faculties

Dean of Graduate Studies and Scientific Research	Dean of Faculty of Science
Palestine Polytechnic University	Bethlehem University
Date	Date

"Identification of a Missense Mutation in *LRP4* Gene in a Palestinian Family with Cenani-Lenz Syndactyly"

by Lama Abbas Juneidi

ABSTRACT

Cenani-Lenz syndactyly is an autosomal-recessive congenital anomaly affecting mainly distal limb development. It is characterized by fusion and disorganization of metacarpal and phalangeal bones, radioulnar synostosis, and severe syndactyly of hands and feet. Here, we report the first case of Cenani-Lenz syndactyly among the Palestinian population. In our study, next-generation sequencing was performed on samples obtained from a large consanguineous family. Causative variant in NGS data was selected through standard bioinformatics tools. Candidate variant was Sanger sequenced in all available family members. Sequence analysis identified the homozygous missense mutation c.3049T>C (p.Cys1017Arg) in exon 22 of the *LRP4* gene among four affected individuals, and perfectly segregated with the phenotype in the rest of the family. The gene *LRP4* belongs to the low-density lipoprotein (LDL) receptor-related protein (LRP) family, which members are essential for various developmental processes. *LRP4* gene is important for the control and modification of Wnt signaling, a pathway that has an important role in limb development. The identified variant is located in the extracellular EGF-like domain of LRP4 and is highly conserved across various species. We propose that this missense mutation will abolish the inhibitory effect of LRP4 and thus will lead to over activation of the Wnt signaling cascade. This variant is predicted to be "pathogenic" by SIFT, Polyphen-2 and Mutation taster software, but functional analyses are still required to further support the causality. Our study will contribute to the understanding of the pathogenesis underlying Cenani-Lenz syndactyly, improving clinical and molecular diagnosis; thus, making genetic counseling and preimplantation genetic diagnosis (PGD) easier in future.

"التعرف على طفرة وراثية في جين *LRP4* و التي*تسبب* متلازمة ارتفاق الأصابع من نوع Cenani-Lenz في عائلة فلسطينية"

لمى عباس الجنيدي

ملخص

إن متلازمة ارتفاق الأصابع من نوع Cenani-Lenz هو خلل جسمي متنحي (autosomal recessive) ناتج عن تشوه خلقي في الأطراف العلوية والسفلية، حيث يتمثل في التصاق عظام مشط اليد (العظام السنعية) و مجموعة عظام السلاميات، مع التحام في عظمتي اليد الزند و الكعبرة، و يحدث نتيجة طفرات وراثية اثناء تكون الجنين و عوامل أخرى. في هذه الدراسة كشفنا عن أول عائلة فلسطينية تعاني من ارتفاق الاصابع من نوع Cenani-Lenz، وقمنا بتحديد العامل الوراثي المسؤول عن هذه المتلازمة في هذه العائلة. خضعت الأسرة -والتي تضم أربعة أشخاص مصابين- لتشخيص تفصيلي ومن بعده فحص المادة الوراثية لجميع الأفراد. كشفت تقنية Next-generation sequencing عن طفرة في الجين *LRP4* ضمن اكسون 22 أدت إلى تغيير الحمض الأميني Cysteine إلى Arginine على موقع 1017 من البروتين. يعد LRP4 من عائلة البروتينات المستقبلة للبروتين الدهني منخفض الكثافة (LRPs)، والتي لها دور هام في تنظيم و تنسيق عمل سبيل Wnt المسؤول عن توصيل الإشارة خلال عملية تكوّن الأطراف، حيث يثبط بروتين LRP4 إشارة Wnt. إن هذه الطفرة تتواجد في نطاق عامل نمو البشرة المتعدد (EGF) من البروتين LRP4، الذي تم حفظه تطوريا في العديد من الكائنات لأهميته. لذلك فإن وجودها في هذا الموقع يمنع من تثبيط مسار Wnt ويزيد من تحفيز هذه الإشارة مسببا خلل في انفصال الأصابع أثناء النمو الجنيني. نتائجنا تساعد في فهم الآليّة البيولوجية لنشوء المرض مما يسهم في تحسين التشخيص الجزيئي ويتيح الفرصة للعائلة لعمل تشخيص وراثي سابق للانغراس (PGD) للحصول على جنين سليم غير حامل للطفرة.

DECLARATION

I declare that the Master Thesis entitled "**Identification of a Missense Mutation in *LRP4* Gene in a Palestinian Family with Cenani-Lenz Syndactyly**" is my own original work, and hereby certify that unless stated, all work contained within this thesis is my own independent research, and has not been submitted for the award of any other degree at any institution, except where due acknowledgment is made in the text.

Name and signature: "Lama A. Juneidi"

Date: _____

STATEMENT OF PERMISSION TO USE

In presenting this thesis in partial fulfillment of the requirements for the joint master degree in biotechnology at Palestine Polytechnic University and Bethlehem University, I agree that the library shall make it available to borrowers under rules of the library. Brief quotations from this thesis are allowable without special permission, provided that accurate acknowledgement of the source is made.

Permission for extensive quotation from, reproduction, or publication of this thesis may be granted by my main supervisor, or in his absence, by the Dean of Higher Studies when, in the opinion of either, the proposed use of the material is for scholarly purposes. Any copying or use of the material in this thesis for financial gain shall not be allowed without my written permission.

Signature: "Lama Abbas Juneidi"

Date: _____

Dedication

I dedicate this thesis to my beloved parents, who have been a great source of inspiration and support throughout my life. Without them, none of my success would be possible. I am forever indebted to you for giving me the opportunities that have made me who I am.

Acknowledgments

I would like to thank my supervisor Dr. Hashem Shahin, who guided me throughout this project. It has been a great honor to work at his lab.

A debt of gratitude is also owed to Dr. Bernd Wollnik for his generous help in doing Next-generation sequencing at The Institute of Human Genetics, University of Göttingen, Germany.

I would like to extend my thanks to Pal-Orthopedics Center for providing detailed phenotyping for the family, and to Prof. Dr. Steven Hovius (Department of Plastic and Reconstructive Surgery, Rotterdam, The Netherlands) for surgery consultation.

I wish to express my special thanks to Prof. Socrates Tzartos (Hellenic Pasteur Institute, Athens, Greece) and Dr. Inga Koneczny (Medical University of Vienna, Vienna, Austria) who kindly provided LRP4-GFP plasmid for future variant validation. I really appreciate their contribution.

Last but not the least, I would like to thank the family members for their cooperation.

Abbreviations

AARRS	Al-Awadi–Raas–Rothschild syndrome
AD	Autosomal Dominant
AER	Apical Ectodermal Ridge
APC	Adenomatous Polyposis Coli
AR	Autosomal Recessive
BAK	B-cell lymphoma 2 homologous antagonist/killer
BAX	B-cell lymphoma 2-associated X
BCL2	B-cell lymphoma 2
BMP	Bone Morphogenic Protein
CK1	Casein Kinase 1
CLS	Cenani-Lenz Syndactyly
Cyp26A1	Cytochrome P450 member 26A1
Dkk	Dickkopf
DNA	Deoxyribonucleic acid
dNTPs	Deoxynucleotide Triphosphates
Dsh	Disheveled
ECD	Extracellular Domain
ECM	Extracellular matrix
EDTA	Ethylenediaminetetraacetic acid
EGF	Epidermal Growth Factor
EtBr	Ethedium Bromide
FGF	Fibroblast Growth Factor
FS	Fuhrmann syndrome
FZD	Frizzled
GREM-1	GREMLIN-1
GSK	Glycogen Synthase Kinase
ICD	Intracellular Domain

LDL	Low-density Lipoprotein
LEF	Lymphoid Enhancer Factor
Lmx1b	LIM-homeodomain factor Lmx1b
LRP4	Low-density lipoprotein receptor-related protein 4
MEGF7	Multiple EGF-like domain 7
MSSD	Mesoaxial Synostotic Syndactyly
NGS	Next Generation Sequencing
NMJ	Neuromuscular Junction
OMIM	Online Mendelian Inheritance in Man
PCP	Planar Cell Polarity
PCR	Polymerase Chain Reaction
PGCs	Primordial Germ Cells
POLYPHEN	Polymorphism Phenotyping
RA	Retinoic Acid
RALDH2	Retinaldehyde dehydrogenase 2
SDS	Sodium Dodecyl Sulfate
SHFM6	Split-Hand/Foot Malformation type 6
SHH	Sonic Hedgehog
SIFT	Scale-invariant feature transform
SNP	Single Nucleotide Polymorphism
SOST2	Sclerosteosis type 2
SPD	Synpolydactyly
TAE	Tris base, acetic acid and EDTA
TCF	T Cell Factor
UV	Ultraviolet
WNT	Wingless-type MMTV integration site
WT	Wild Type
XLR	X-Linked Recessive
ZPA	Zone of Polarizing Activity

List of Figures

List of Tables

Table of Contents

CHAPTER 1

Introduction

The limb is a complexly patterned organ. It originates from the lateral plate mesoderm and develops along three major axes, each of which is controlled by a different signaling center (Petit et al. 2017). In the developing limb bud, fingers become apparent at day 41–43 and are fully separated at day 53.5. Apoptosis is needed for separation of the fingers. Multiple signaling pathways mediate this process (Montero et al. 2020). Hence, any disturbance during differentiation and morphogenesis of structural limb tissues will lead to limb deformities.

Congenital limb malformations occur in 1 in 500 to 1 in 1000 human live births and are diverse in their epidemiology, etiology and anatomy (Malik 2012). The molecular analysis of disturbed gene function in inherited limb malformations provides essential information for the understanding of physiological and pathophysiological limb development in humans, as well as in other vertebrates (Petit et al. 2017). Non-syndromic syndactyly is one of the most common congenital deformities, a heterogeneous hereditary condition of webbed fingers and/or toes with an incidence of 1 in 2000-3000 live births (Malik 2012). The malformation can be unilateral or bilateral, and the fusion within the web may be cutaneous or bony. The phenotype varies in families, and intra-familial variability is also quite common. The majority of syndactylies show autosomal dominant mode of inheritance, with variable expression and incomplete penetrance (Umair et al. 2018).

Cenani-Lenz syndactyly is an autosomal recessively inherited disorder (Cenani and Lenz 1967). The phenotype is characterized by bilateral hand and foot syndactyly with or without oligodactyly. It includes a range of partial to complete fusion of the carpals, metacarpals, or phalanges. In more severe cases, radioulnar synostosis and mesomelic shortening may be present, along with other

variable facial and systemic features. The lower limbs are typically less severely affected than the upper limbs (Al-Qattan and Alkuraya 2019). Cenani-Lenz syndactyly is known to be associated with specific *LRP4* variants (Li et al. 2010).

The Low-density lipoprotein receptor-related protein 4 (LRP4) protein, is a member of the highly conserved LDL receptor-related protein (LRP) family which has diverse functions in developmental processes, lipoprotein trafficking and cell signaling (May et al. 2007). One of the pathways in which LRP4 and other members of the LDLR-related protein family are involved in, is the Wnt signaling pathway (Teufel and Hartmann 2019). Wnt is known to be involved in numerous aspects of embryonic development. Binding of WNT ligands to LRP5 and LRP6 leads to the stabilization of β-catenin and subsequent transcriptional activation of Wnt target genes (Ng et al. 2019). Limb malformations are thought to be caused by abnormal Wnt and β-catenin signaling in the developing limb bud (Baron and Kneissel 2013). LRP4 was shown to inhibit LRP6/LRP5-mediated activation of canonical Wnt signaling (Li et al. 2010; Tian et al. 2019). Loss of LRP4 function leading to excessive Wnt and β-catenin signaling underlies the pathogenesis of Cenani-Lenz Syndactyly (Al-Qattan 2019).

In the present study, we report a large consanguineous family diagnosed with Cenani-Lenz syndactyly for the first time among Palestinian population. Genetic testing for the affected individuals was performed via Next generation sequencing followed by bioinformatics analysis and Sanger sequence validation. Results revealed a missense substitution in *LRP4* gene. These cases further contribute to the phenotypic spectrum seen in Cenani-Lenz syndactyly, and support earlier reports of genotype–phenotype correlations, and showcase the utility of next generation sequencing in genetic counseling situations.

CHAPTER 2

Cenani-Lenz Syndactyly Syndrome

2.1 Syndactyly

2.1.1 Historical Background

The term syndactyly is derived from the Greek word “Syn” meaning together and “Dactylos” meaning digits. One of the earliest records of syndactyly as a birth defect is referred to a famous Andalusian surgeon in the Middle Ages named Abu Alkasem Al-Zahrawi (Albucasis) (Al-Zahrāwī et al. 1973). Albucasis described syndactyly as a condition resulting from either a congenital disorder or a healing wound. He reported the various presentations of this anomaly and possible treatments (Asaad et al. 2019). Another worth mentioning surgeon is Ambroise Pare, who described syndactyly in the 16th century as fingers stuck together (Bell 1953). Later on, syndactyly started to appear in the literature under different terms. For example, adherent fingers, fingers coated with common skin, coherence of fingers, fingers grown together, fingers knit together, skin fusion, digits in stocking, fingers stuck together, syndactylous, syndactylia, syndactylous ossification, webbed toes, and zygodactyly (Malik 2012).

Syndactyly has long been believed to have a genetic component, and it has been researched greatly over the last decade. Many studies on developmental biology and embryology of the upper limb have improved our understanding of the genetics and the phenotypes of this congenital limb abnormality. Molecular genetics has played an essential role in delineating the basic mechanisms of this disease and allowed for accurate and proper diagnosis and selecting for a suitable treatment and future rehabilitation afterwards, and even provided benefits that lie beyond the affected individuals (Jordan et al. 2012).

2.1.2 Significance

Syndactyly is one of the most common congenital malformation of the limbs, with an incidence of 1 in 2000-3000 live births (Malik 2012). It is more common in males than females with a ratio of 2:1, and bilateral involvement is found in approximately half of cases (Rayan and Upton III 2014). Syndactyly has also been found to be prevalent among Arab populations; it has been reported either as an isolated clinical phenotype or as a feature of syndromic malformations (Abu-Libdeh and Teebi 2010).

2.1.3 Etiology

Syndactyly mainly occurs due to the lack of apoptosis in the mesenchyme of the tissues between the limb digits. This failure of differentiation between adjacent digits starts at the seventh and eighth weeks of embryonic life, when no distinct cartilaginous entities are formed, resulting in the fusion of limb bones, rather than being normally separate from one another (Al-Qattan 2019). This whole process is under the influence of several encoding proteins and transcription factors involved in limb formation (some of which will be discussed in subsequent sections), so genetic analysis has found that syndactyly phenotypes do not appear to be one gene specific, but rather dependent on a wide range of genes (Al-Qattan and Alkuraya 2019).

However, sporadic syndactyly with no familial history could be associated with environmental factors in-utero that predispose the fetus to syndactyly and other congenital hand abnormalities. Man and his colleagues performed a study which linked maternal smoking and syndactyly occurrence (Man and Chang 2006). Another study suggested that low nutritional status during early pregnancy and working condition before pregnancy could also contribute to the development of polydactyly and syndactyly (Luo et al. 2009).

2.1.4 Classification

2.1.4.1 Classification Schemes Proposed For Syndactyly

As the number of reported cases regarding syndactyly as a congenital deformity increased into the medical records, it required a systematic evaluation of the various types. Therefore, several attempts were made to classify the webbing of digits. Depending upon the approach taken, syndactyly classification could fall into three categories. Scientists started with the simple anatomical approach (Bell 1953; Leonard Goldner 1975). Based on the extent of webbing and the number of digits involved, syndactyly has been categorized into partial vs complete type. Another category considers descriptive and embryological approaches of classification (Swanson 1976); these approaches rely on the grouping of similar patterns of limb deficiencies due to embryological failures. For instance, based on failure of differentiation, syndactyly could be classified as simple vs complicated (Swanson 1976). This approach also takes into consideration if the deformity involves soft/skeletal tissue or only the dermal structure, as well as the mechanism of pattern formation and secondary modeling of limb bud during development. Hence, they categorize syndactylies as pre-axial, meso-axial, post-axial, and total webbing types (Winter and Tickle 1993). One of their main objectives has been to help choosing the best surgical treatment to restore the correct digit number, size of individual rays, and digit shape (Foucher et al. 2001). The third approach of classification is the clinical genetic approach, which was first proposed by Temtamy and McKusick (Temtamy and McKusick 1978), their classification is essentially based on the phenotypic presentation (site and nature of digit involvement) and the pattern of disease inheritance in large families. They were able to identify five discrete and isolated syndactylies, in addition to a few unclassified types. Since then it has been the most widely used classification scheme by the geneticists and clinicians, and the OMIM catalogue has adopted it.

2.1.4.2 Current Classification

The limb malformation could be either isolated (non-syndromic) or associated with other organ dysfunction or malformation as a part of a syndrome (syndromic) (Ahmed et al. 2017). Syndromic syndactylies involve many different disorders, and here we will only focus on the classification of the non-syndromic syndactyly types. The current classification scheme of syndactyly is an adaptation and extension of Temtamy-McKusick classification system mentioned earlier but with introducing into it the clinical, genetic, and molecular developments in this field (Malik 2012). The syndactyly types identified according to the current classification are nine distinct types with some variations and sub-divisions described in (Table 2.1, Figure 2.1) (Umair et al. 2018).

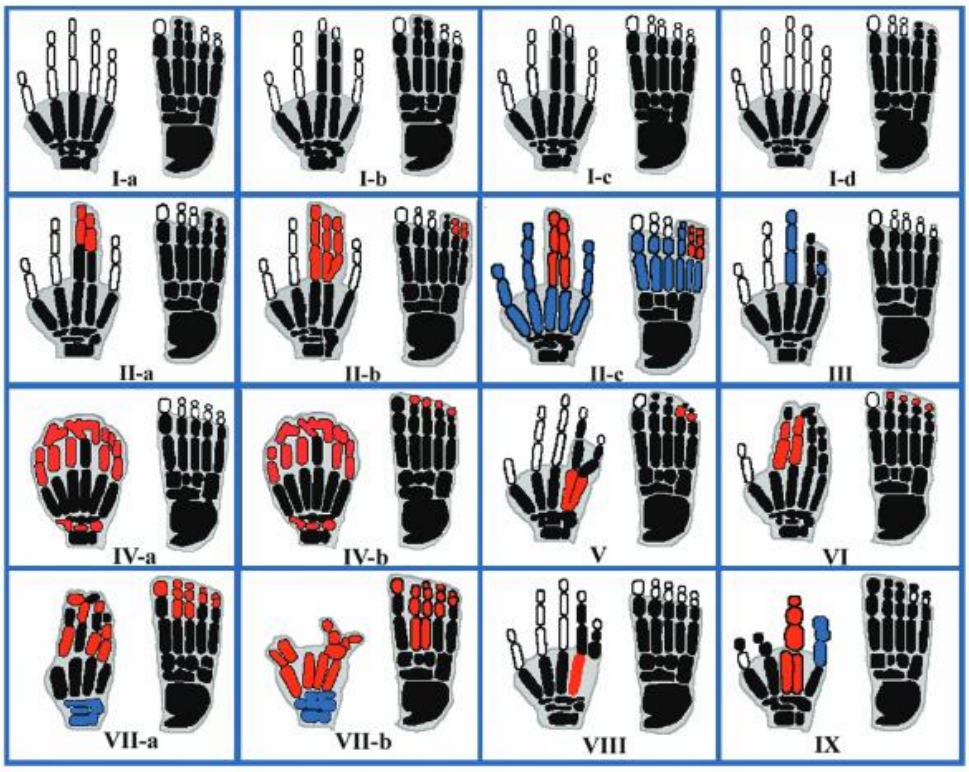

Figure 2.1: Cartoon representation of non-syndromic syndactyly types. Red portion represents synostosis and blue region represents clinodactyly and other abnormalities (Umair et al. 2018).

Table 2.1: Current classification of well-characterized non-syndromic syndactyly types

ID	Type	OMIM	Inheritance	Gene	References
I-a	ZD1; Zygodactyly;	609815	AD	-	(Malik et al. 2005b)
I-b	SD1; Lueken type	185900	AD	-	(Bosse et al. 2000)
I-c	Montagu type	-	AD	*HOXD13*	(Dai et al. 2014)
I-d	Castilla type	-	AD	-	(Malik 2012)
II-a	SPD1; Vordingborg type	186000	AD	*HOXD13*	(Muragaki et al. 1996)
II-b	SPD2; Debeer type	608180	AD	*FBLN1*	(Debeer et al. 2002)
II-c	SPD3; Malik type	610234	AD	-	(Malik et al. 2006)
III	SDTY3	186100	AD	*GJA1*	(Paznekas et al. 2003)
IV-a	SDTY4; Haas type	186200	AD	*ZRS(LMBR1)*	(Wu et al. 2009)
V	SDTY5	186300	AD	*HOXD13*	(Zhao et al. 2007)
VI	Mitten type	-	AD	-	(Temtamy and McKusick 1978)
VII-a	Cenani-Lenz type	212780	AR	*LRP4*	(Li et al. 2010)
VII-b	Oligodactyly type	-	AD	*FMN1-GREM1*	(Dimitrov et al. 2010)
VIII-a	Orel-Holmes type	309630	XLR	*FGF-16*	(Jamsheer et al. 2013)
IX	MSSD; Malik-Percin type	609432	AR	*BHLHA9*	(Malik et al. 2005a)

Abbreviations: AR = autosomal recessive, AD = autosomal dominant, XLR = X-Linked recessive

2.1.5 Syndactyly Pathway of Pathogenesis

In humans, the normal separation of digits starts at embryonic stage 19 and ends at stage 22 (Hill and Lettice 2016). Normally, the spaces between digits are formed due to cell death at this area (interdigital cell death), together with the extracellular matrix degradation (Al-Qattan 2014). These events are controlled by a process called epithelial–mesenchymal feedback signaling; which is a loop between an important pathway known as sonic hedgehog (SHH), and a strong suppressor of the bone morphogenetic proteins BMP signaling called gremlin1 (GREM1), and fibroblast growth

factor 8 (FGF8) (Verheyden and Sun 2008). Before stage 19 of embryonic life, the digits are normally webbed. During this time, high levels of SHH signaling stimulate the expression of GREM1, which in turn inhibits BMP signaling in the interdigital mesoderm leading to a high level of FGF8 in the interdigital ectoderm. FGF8 inactivates retinoic acid activity preventing apoptosis, this will ensure that the digits are normally maintained in the webbed state (Figure 2.2A) (Al-Qattan 2014). On the other hand, during the growth of hand paddle at stages 19–22, the cells will leave the zone of polarizing activity (which is the area that contains signals that instruct the developing limb bud to grow along the anterior/posterior axis) to contribute to the posterior digits. These cells will no longer express SHH, hence, GREM1 will not be stimulated. The loss of GREM1 from the interdigital mesoderm leads to up-regulation of BMP signaling and suppression of FGF8 (Figure 2.2B). The reduction in FGF8 activity will finally allow retinoic acid to initiate apoptosis of cells in the interdigital space, and web separation (Al-Qattan 2014).

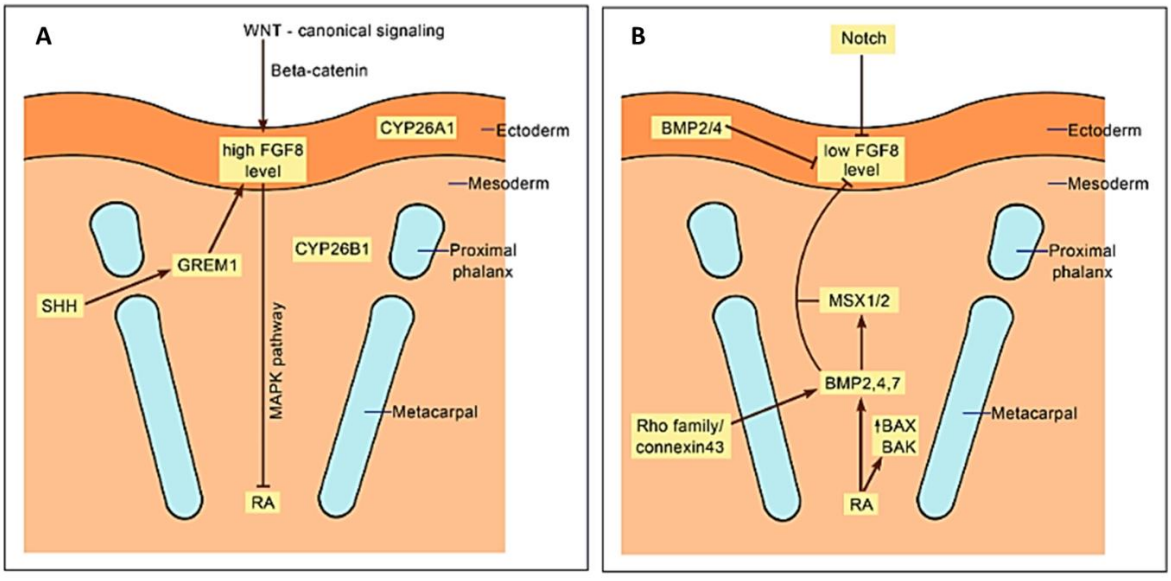

Figure 2.2: **Molecular biology of the interdigital area**. **A)** Before the onset of web creation, (SHH-GREM1–FGF8) signaling ensures high FGF8 levels in the ectoderm, low BMP activity in the mesoderm, and inactivation of retinoic acid RA. **B)** During web creation, low levels of FGF 8 in the ectoderm, high BMP levels in the ectoderm and mesoderm, and high RA activity in the mesoderm (Al-Qattan 2014).

Therefore, syndactyly is produced by any event that leads to persistent expression of GREM1 within the mesoderm or persistent high FGF8 activity within the mesoderm and ectoderm, which will eventually cause failure of digits separation. Al-Qattan has summarized the pathogenesis of almost all types of syndactyly into 3 major steps (Figure 2.3), based on the molecular pathways involved in human and animal models of syndactylies (Al-Qattan 2019).

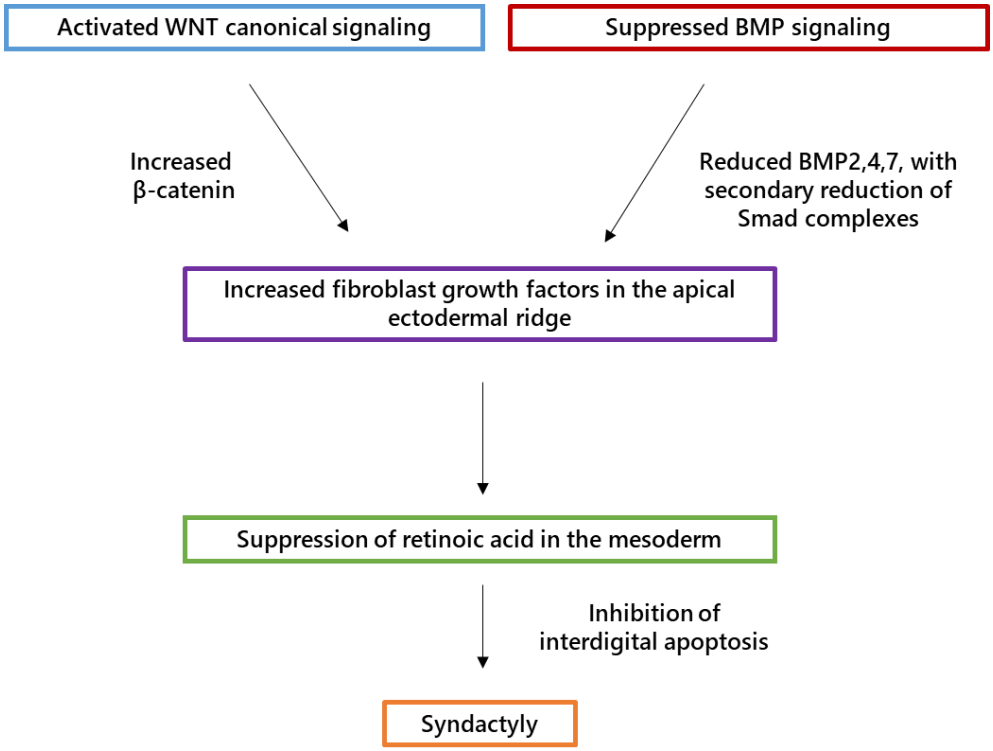

Figure 2.3: The main pathophysiological cascade of events leading to syndactyly (Al-Qattan and Alkuraya 2019).

2.1.5.1 Step 1

The first step is either the activation of the WNT canonical signaling or the suppression of the Bone Morphogenetic Protein (BMP) canonical signaling. In humans, gene mutations that lead to disruptions of these events will cause syndactyly. One example is the loss of function mutations in *GJA1* gene, which in turn lead to reduced BMPs and syndactyly type 3 (Paznekas et al. 2003). Of special importance, is the WNT signaling, which will be discussed in detail in Chapter 3.

2.1.5.2 Step 2

Increased activity of fibroblast growth factor 8 (FGF8) is the key middle step mediating the pathogenesis of syndactyly. FGFs function by binding and activating their specific cell surface tyrosine kinase receptors. FGF8 will bind to its receptor, activating intracellular pathways known as mitogen-activated protein kinases (MAPK) pathway (Turner and Grose 2010). The MAPK pathway is a chain of proteins in the cell that communicate a signal from a receptor to the DNA. The pathway includes several kinases that add phosphate groups to proteins, which either activates or inactivates them. In our case, high level of ectodermal FGF8 acts as a diffusible morphogen within the mesoderm, which will inactivate retinoic acid via MAPK pathway (Al-Qattan 2019).

2.1.5.3 Step 3

The final step in the pathway is the suppression of retinoic acid in the mesenchyme, which will lead to the suppression of both apoptosis and extracellular matrix (ECM) degradation. The question is how does retinoic acid induce apoptosis? Retinoic acid (RA) is formed when the enzyme retinaldehyde dehydrogenase 2 (RALDH2) oxidizes retinol (vitamin A) to retinoic acid. Retinoic acid functions as a ligand for nuclear retinoic acid receptors, and it was shown that it has responsive elements in the promoter regions of members of the Bcl-2 gene family known as Bcl-2-associated X protein (BAX) and Bcl-2 homologous antagonist/killer (BAK) which act as pro-apoptotic regulators. Hence, RA up-regulates BAX and BAK, and apoptosis is thus induced (Díaz-Hernández et al. 2014). One might wonder why does retinoic acid induce apoptosis within the interdigital space and not within the digits themselves, Zhao et al. answered this question by showing that the digits express a cytochrome called Cyp26b1 which inactivates retinoic acid. Hence, mesodermal retinoic acid is unable to degrade the digits (Zhao et al. 2010).

2.1.6 Genetic Basis of Syndactyly

The genetic factors involved in causing syndactyly fall into four major groups: 1) Mutations in genes encoding transcription factors that are responsible for growth and skeletal tissue differentiation; such as Fingerin, HoxD13, BHLHA9 (Kataoka et al. 2018). (2) Mutations in cell adhesion and extracellular matrix components; among these are integrins alpha 3 and 6, laminin alpha 5, fibrillin 2, fibulin 1, and metalloproteases (Debeer et al. 2002). (3) Mutations that cause dysregulation of the signaling pathways important in the digits morphogenesis; including BMP signaling, FGF signaling, Notch signaling, TGF beta signaling, Hedgehog signaling and Wnt signaling (Maupin et al. 2013). 4) Alterations in the cell degradation machinery such as mutations in BAX and BAK genes (both encode pro-apoptotic proteins) (Montero et al. 2020).

2.1.7 Mode of Inheritance

Syndactylies vary in their patterns of inheritance, most of the syndactyly types are inherited as autosomal dominant but two types are autosomal recessive, and one X-linked recessive entity has also been described (Table 2.1).

2.1.8 Complexity

There are various factors that complicate the understanding of syndactyly. For instance, syndactyly displays genetic heterogeneity; meaning that mutations of different genes can lead to the same phenotype (e.g., type II syndactyly) (Malik et al. 2006). Conversely, mutations in the same gene can lead to different phenotypes (e.g., HOXD13) (Dai et al. 2014; Deng et al. 2017). It is still unknown how the same underlying genetic factors may lead to dissimilar webbing in hands and feet.

This complexity is even amplified by the fact that each syndactyly can also exist in a range of more than 300 distinct syndromic syndactylies. Intra-familial and individual-specific clinical variability may result in phenotypic overlap with other entities, since the same individual may exhibit asymmetrical phenotypes in the upper and lower, and right and left limbs. (Ahmed et al. 2017).

Furthermore, some syndactyly phenotypes demonstrate widely variable expressivity and incomplete penetrance (Malik 2012). One factor that might contribute to their reduction is somatic mosaic mutations (occurs when different genotypes arise from a single fertilized egg cell, due to mitotic errors). A study group has identified a mosaic somatic mutation in the *PIK3CA* gene in a patient affected with syndactyly, the mutation was present in the syndactylous tissue, but not in the peripheral blood (Tripolszki et al. 2016).

Moreover, the typing of syndactyly can even be more puzzling due to limited number of families linked to each syndactyly locus (Malik 2012). Also, there is a large number of morphogens that are involved in limb development with many complex interactions between these morphogens. In addition to the involvement of modifier genes and long range regulatory elements (Petit et al. 2017). These complex signaling cascades need to be maintained in an appropriate signal equilibrium to insure growth and differentiation of limb tissue. One syndactyly type that is caused by an abnormal balance between signaling molecules is known as Cenani-Lenz syndactyly.

2.2 Cenani-Lenz Syndactyly

2.2.1 Overview

Cenani-Lenz syndactyly (CLS) was first described in 1967 by the Turkish scientist Cenani and his German colleague Lenz (Cenani and Lenz 1967), who studied two brothers with an Apert syndrome-like form of syndactyly. However, their unusual finding was that they noted severe bony

fusion of all hand digits, to such an extent that no phalangeal element was identifiable which made them report a new disorder and named it after them (Cenani and Lenz 1967).

Cenani-Lenz syndrome is a very rare phenotype caused by a disordered axial and longitudinal differentiation of the upper and/or lower limbs. Two different clinical phenotypes of CLS seem to exist; the classical type which is mainly characterized by a total syndactyly of the hand (so called spoon hands), and the other is an oligodactyly type (Harpf et al. 2005).

In 1994, Cenani-Lenz syndactyly has been introduced to syndactyly types classification, and listed as Syndactyly Type VII by Goldstein, who has extended the previous Temtamy-McKusick classification (Temtamy and McKusick 1978) and added three additional types (Goldstein et al. 1994).

2.2.2 Inheritance and Clinical Features

The mode of inheritance of Cenani-Lenz syndactyly is autosomal recessive. Temtamy et al. once reported a CLS family with quasidominant inheritance, in which the inheritance of a recessive trait mimics a dominant pattern (pseudodominance) (Temtamy et al., 2003). Despite the differences among patients, the main features of Cenani-Lenz syndactyly that are found in almost all of the reported cases are complete syndactyly of the hands associated with disorganization of metacarpals and phalanges, and variable fusion of the radius and ulna (Malik 2012). Some patients suffer from a number of complications including kidney malformation (Bacchelli et al., 2001; Jarbhou et al., 2008; Kariminejad et al., 2013; Li et al., 2010) others were found to develop hearing loss (Seven et al. 2000; Dimitrov et al. 2010). Less frequent malformations include facial dysmorphism (Jarbhou et al. 2008), hypothyrodism, and genital abnormality (Temtamy et al. 2003). Recently, recurrent ketotic hypoglycaemia was reported in two affected brothers originating from a small

Orthodox Jewish community in the Yemen, which has not been associated with Cenani-Lenz phenotype previously (Steel et al. 2020).

2.2.3 Genetic Heterogeneity

It was not until 2010, that the study group Li et al. did discover the causative gene for Cenani-Lenz syndactyly. Li et al published a landmark paper demonstrating the use of genome-wide linkage analysis in six consanguineous CLS-affected families to be the first who map the CLS locus. They identified the low-density lipoprotein (LDL) receptor-related 4 (*LRP4*) gene, as the gene responsible for the majority of CLS cases (Li et al., 2010). After homozygosity mapping, they continued the molecular analysis of *LRP4* in all the previously reported families (14 families in total) who originate from Egypt, Turkey, Pakistan and Jordan. They were able to identify homozygous and compound heterozygous missense mutations and splice mutations in 12 families (Li et al., 2010).

Genetic heterogeneity of CLS was evident by the failure to identify *LRP4* mutations in two of the well-phenotyped 14 families used to map the disease locus, and by lack of linkage to *LRP4* in at least one of these two families. In another molecular study, Patel et al. described an extended consanguineous CLS family in which they mapped the disease to a novel locus that harbors a splicing mutation in the Adenomatous polyposis coli gene (APC), implicating APC for the first time in the pathogenesis of this syndactyly (Patel et al. 2015).

More interestingly, Cenani–Lenz phenotype might be due to genomic rearrangements of *GREM1-FMN1* locus on chromosome 15q13.3 (Dimitrov et al. 2010). However, this phenotype differs from the classical CLS in that it segregates in an autosomal dominant manner, and it is manifested with oligodactyly together with renal defects and hearing loss (Harpf et al. 2005).

CHAPTER 3

The Wnt Signaling Pathway in Limb Development

3.1 Vertebrate Limb Development

The developing limb bud is an outgrowth of somatic mesoderm and lateral plate mesoderm into the overlying ectoderm. The time of appearance of the bud is at embryonic stage 12, which is equivalent to 26 days after fertilization (Petit et al. 2017). To simplify the process, when a secreted protein binds to its receptor, it leads to intracellular changes, and activate specific transcription factors that carry the signal to the nucleus of the cell, then bind to DNA and lead to expression of new target genes. During the outgrowth, the limb is patterned into three axes: the proximal-distal (PD) (from shoulder to digit tip), the anterior-posterior (AP) (from thumb to small finger) and the dorsal-ventral (DV) (from the dorsum to the palm of the hand) axis under the influence of different signaling centers (Petit et al. 2017).

Induction of limb development starts when the neighboring cells start secreting one of the fibroblast growth factors FGF8, which induces FGF10. Once FGF10 is induced, it activates the ectodermal cells from where the budding will start. This will allow the cells to start proliferating and will establish what is called the apical ectodermal ridge (AER) (Hill and Lettice 2016). The AER is a thickened epithelial structure that functions as an organizing center for limb bud development and controls the outgrowth and the patterning of the proximal-distal axis. With the help of T-box family transcription factors TBX4 and TBX5 activate FGF10 (Ng et al. 2002), which activates the secretion of a WNT signaling component *WNT3A*, which in turn sustains the AER's expression of FGF8, creating a positive feedback loop between the AER and limb mesenchyme.

Thus, the AER keeps the mesenchyme in a proliferative state, allowing the limb to grow (Figure 3.1A) (Petit et al. 2017).

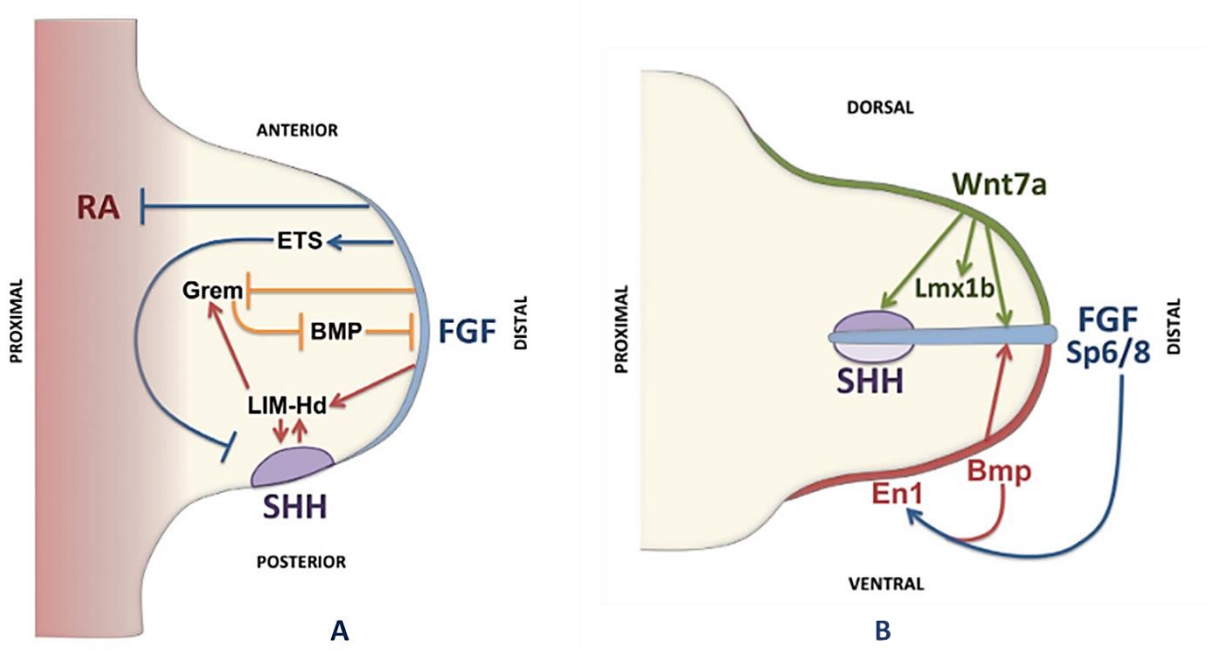

Figure 3.1: The molecular pathways involved in the developing limb bud. A) The expression of FGFs forms the AER. FGFs from the AER together with retinoic acid induce the expression of SHH in the ZPA. The FGF-SHH positive feedback loop maintains AER and ZPA activity. **B)** Dorsal-ventral patterning in the limb bud ectoderm regulates AER positioning and promotes SHH that is maintained by *WNT7a*. BMP signaling activates engrailed *En1*, which restricts *Wnt7a* to the dorsal ectoderm. *WNT7A* activates *Lmx1b* and contributes to SHH activation in the mesenchyme (Delgado and Torres 2017).

The FGFs secreted by the AER help in establishing a second signaling center known as zone of polarizing activity (ZPA), which controls the anterior-posterior axis. ZPA is a group of limb mesenchymal cells located in the posterior limb bud margin (Al-Qattan et al. 2009). Formation of the ZPA depends on the expression of *HOXB-8* gene and retinoic acid in the posterior mesoderm. The master player in the ZPA is the expression of a vertebrate hedgehog family member called sonic hedgehog (SHH), which is up-regulated in the ZPA through retinoic acid (Carballo et al. 2018). The development of the AP axis is mainly mediated through the expression of sonic

hedgehog (SHH) morphogen. Digits 3, 4 and 5 are specified by a temporal gradient expression of SHH. Digit 2 is specified by a long-range diffusible SHH form and digit 1 does not require SHH (Tickle and Towers 2017). The FGF signaling from the AER is required for SHH expression, whereas SHH signaling is required to maintain the AER integrity, which is accomplished in a complicated set of positive and negative feedback loops (Figure 3.1A) (Petit et al. 2017).

Finally, the dorsal-ventral axis is thought to be regulated by WNT family member 7A (WNT7A) signaling in the overlying ectoderm (Figure 3.1B). WNT7a is one of the factors responsible for the preservation of the SHH signal in the ZPA (Lan et al. 2019). It was shown that WNT7a induces the expression of the LIM-homeodomain factor *LMX1B*, which encodes a transcription factor that is both, necessary and sufficient to determine dorsal limb bud identity. Hence, all the dorsal features and structures of the hand and digits including the nails are mediated by Wnt pathway. The BMPs in the ventral ectoderm expresses Engrailed 1 *(EN-1*) gene, which represses *WNT7a* activity and restricts its effect to the dorsal ectoderm (Ball et al. 2021).

3.2 The Wnt Signaling Pathway

Wnt signaling cascade is a highly conserved cellular communication pathway across species ranging from nematodes to mammals (Holstein 2012). It plays important roles during embryonic development including cellular differentiation, cell proliferation and migration, as well as body axis patterning (Nusse and Clevers 2017; Wiese et al. 2018). The first *WNT* gene was identified in 1982 by the two scientists Roel Nusse and Harold Varmus (Nusse and Varmus 1982). They infected mice with mouse mammary tumor virus to find out which genes will induce breast cancer. This has led to the identification of a new proto-oncogene, which was named by that time *integrated-1* or *int-1*. Later, it was shown that *int-1* gene in mouse has a homologous gene in

Drosophila called *wingless* gene (*wg*) (Rijsewijk et al. 1987), which controls segment polarity and involved in the formation of the body axis during larval development (Nüsslein-volhard and Wieschaus 1980). Thus, the name *Wnt* originates from a combination of *integrated-1* and *wingless* genes and stands for "Wingless-related integration site" (Nusse et al. 1991).

What is unique about Wnt signaling proteins compared to other signals is that they induce asymmetrical cell division, which leads to changes in the cytoskeleton and the mitotic spindle of the cell. This will eventually maintain the correct shaping of the tissues, and generate organized body plans rather than amorphous structures (Teufel and Hartmann 2019).

The Wnt signaling cascade can be divided into The Canonical Wnt pathway, which is β-catenin-dependent pathway, and two additional β-catenin- independent pathways; the Planar Cell Polarity pathway and the Wnt/Ca2+ pathway (Logan and Nusse 2004).

3.2.1 The Canonical Wnt Signaling Pathway

The major player in activating the canonical Wnt cascade is the transcription factor β-catenin. β-catenin is constantly manufactured by the cell, but it is rapidly degraded except when the Wnt pathway is activated (Nusse and Clevers 2017). In the absence of a suitable Wnt ligand, cytoplasmic β-catenin is eliminated by a complex of proteins called the destruction complex, which is composed of the scaffolding protein axin, the tumor suppressor adenomatosis polyposis coli gene product (APC), protein phosphatase 2A (PP2A), and two kinases, casein kinase 1 (CK1) and glycogen synthase kinase 3 (GSK3) (Ng et al. 2019). β-catenin is first phosphorylated by the two kinases on four serine/threonine residues in its amino-terminal region, this phosphorylation makes it a target for ubiquitination by E3 ubiquitin ligase complex and further proteasomal degradation, maintaining the cytosolic and nuclear levels of β-catenin very low (Ng et al. 2019).

When the Wnt pathway is activated, the level of cytoplasmic β-catenin protein is elevated. The activation starts from binding of a Wnt ligand to a transmembrane receptor known as Frizzled (Fz) and to the co-receptors LRP5/6 (members of the low density lipoprotein receptor-related family) (Logan and Nusse 2004; Clevers 2006). After binding to the receptor complex, the Wnt signal is first transduced to a cytoplasmic protein Dishevelled (Dsh), this will induce the phosphorylation of LRPs by the two kinases GSK3 and CK1, resulting in the recruitment of Axin to bind to the phosphorylated LRPs pulling it away from the destruction complex (Ng et al. 2019). As a consequence, the destruction complex is no longer active, leading to a stable β-catenin that will accumulate and translocate into the nucleus, where it binds to transcription factors; T-cell factor (TCF) and lymphoid enhancer-binding factor (LEF) to regulate the transcription of Wnt target genes (Huybrechts et al. 2020). These target genes then control many developmental processes such as posterior patterning, heart, lung, kidney, skin and bone formation (Teufel and Hartmann 2019).

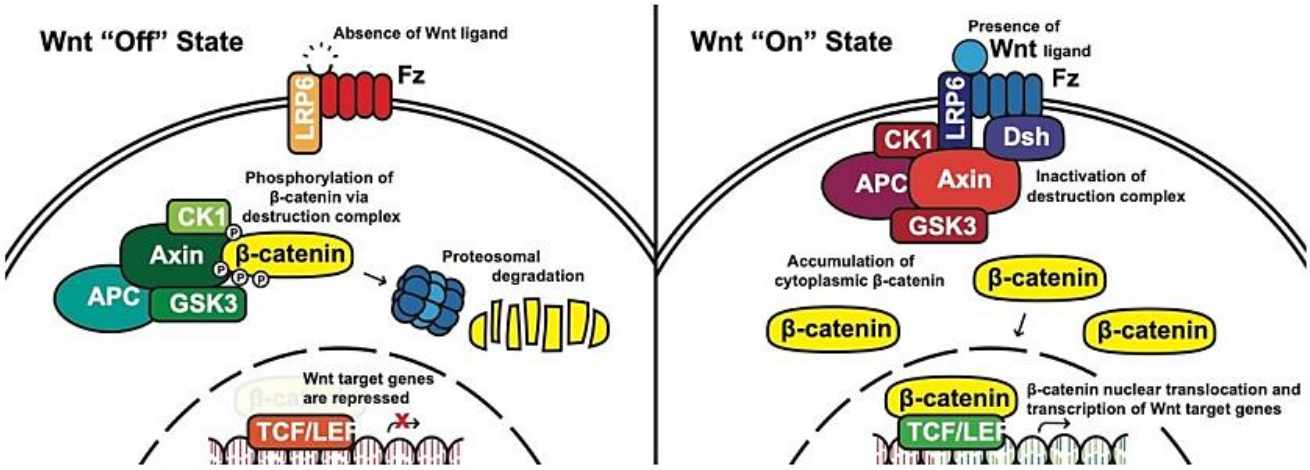

Figure 3.2: The canonical Wnt pathway in on and off states. In the inactive state, without a Wnt ligand β-catenin is phosphorylated by a glycogen synthase kinase 3 (GSK3)-Axin-casein kinase 1 (CK1)–adenomatous polyposis coli (APC) complex and subsequently ubiquitilated and degraded by the proteasome**.** In the active state, binding of Wnt proteins to receptor complex, formed by low-density

lipoprotein (LDL)-related receptor (LRP)5/6 and Frizzled (FZD), will prevent the destruction of β-catenin and thus it will accumulate in the cytoplasm and translocate to the nucleus where it binds to TCF/LEF and induces the expression of target genes (Ng et al. 2019). APC, adenomatous polyposis coli; CK1, casein kinase 1; GSK3, glycogen synthase kinase 3; TCF/LEF, T-cell factor/lymphoid enhancing factor; LRP6, lipoprotein receptor related protein 6; FZD/Fz, Frizzled; Dsh, Disheveled.

3.3 Wnt Signaling Role in Limb Development

Wnt signaling has an essential role in the developing limb bud and controls multiple processes including limb patterning and limb morphogenesis (Teufel and Hartmann 2019). Witte and his colleagues studied the expression of Wnt signaling in the mouse embryos during limb development and cartilage differentiation. They profiled 19 Wnt proteins and revealed highly regulated expression of each of them (Witte et al. 2009). Many of the Wnt genes are highly expressed in the apical ectodermal ridge such as Wnt3, Wnt4, Wnt6, Wnt7a, Wnt7b, Wnt9b, Wnt10a, Wnt10b and Wnt16a (Witte et al. 2009). Of special importance is Wnt3, since it induces the expression of FGF10 and FGF8 and leads to a positive feedback loop between these three components, which is required for AER maintenance and the proximal-distal limb outgrowth (Barrow et al. 2003).

Moreover, Wnt signaling is important in determining the dorsal-ventral limb identity. As aforementioned, Wnt7a is highly expressed in the dorsal limb ectoderm and it controls dorsal-ventral patterning by regulating the expression of *LMX1B*, a factor which determines the dorsal mesodermal cell fate in the limb (Lan et al. 2019). In addition, Wnt7a signaling also regulates the expression of SHH in the ZPA, since there is a positive feedback loop between SHH and FGF4 in the AER (Lan et al. 2019).

Furthermore, during limb morphogenesis Wnt signaling helps in determining the position and morphology of limb structures, such as muscles, tendons and skeletal elements (Teufel and Hartmann 2019). For instance, Wnt11 is expressed in the periphery of the limb mesoderm and is

involved in muscle fiber differentiation whereas Wnt5a triggers muscle fiber specification (Yang 2003).

Finally, Wnt signaling is also involved in bone formation by regulating chondrogenic differentiation from mesenchymal progenitors as well as osteoblast proliferation (Baron and Kneissel 2013). Wnt5a for example was found to promote chondrocyte differentiation in the distal limb bud (Maeda et al. 2019).

3.4 Limb Phenotypes due to Defective Wnt Signaling

Mutations in any component of the Wnt signaling pathway have been shown to cause a variety of limb malformations (Maupin et al. 2013). For instance, a homozygous nonsense mutation in the *WNT3* gene has been found in an extremely rare autosomal recessive congenital disorder called tetra-amelia (OMIM: 273395), which is characterized by the absence of all four limbs accompanied by cleft palate, and pelvic hypoplasia (Niemann et al. 2004). Another important member of the Wnt family is the *WNT5A* gene. It regulates critical morphogenic events, including embryonic patterning and cell differentiation. Heterozygous loss-of-function mutations in the *WNT5A* gene are associated with an autosomal dominant syndrome called Robinow syndrome (OMIM: 180700), which is a disease characterized by skeletal abnormalities including short stature, brachydactyly (meaning shortness of the fingers and toes), abnormal ribs and typical facial dysmorphisms (White et al. 2018). In addition to this finding in humans, heterozygous *Wnt5a* knockout in mice showed a significant decrease in bone resorption due to reduced number of osteoclasts (Maeda et al. 2012). Furthermore, nucleotide changes in *WNT7A* gene cause two distinct disorders manifested by limb malformations. One is Al-Awadi–Raas–Rothschild syndrome (AARRS) (OMIM: 276820) which results in the absence of the ulna and fibula and severe limb deficiencies including truncated limbs and loss of digits (Kantaputra et al. 2010). The

second is called Fuhrmann syndrome (FS) (OMIM: 228930), which is a less severe phenotype but causes bowing of the femurs, aplasia or hypoplasia of the fibula, and poly-, syn-, or oligo-dactyly (Woods et al. 2006). This implicates the essential role of *WNT7A* in limb development as it is expressed in the dorsal ectoderm and involved in the formation of the dorsal-ventral axis, and also maintains sonic hedgehog (SHH) expression that leads to anterior-posterior patterning (Lan et al. 2019). Bi-allelic mutations in the *WNT10B* gene, a key regulator for osteogenesis, cause split-hand/foot malformation type 6 (SHFM6) (OMIM: 225300), which presents with syndactyly, median cleft of the hands and feet, aplasia or hypoplasia of the phalanges, metacarpals and metatarsals (Al-Ghamdi et al. 2020).

CHAPTER 4

LRP4 Gene and its Role in Cenani-Lenz Syndactyly

4.1 *LRP4* Gene: Structure and Function

LRP4 gene (OMIM: 604270) encodes a member of the low-density lipoprotein (LDL) receptor-related family, which consists of many evolutionarily conserved transmembrane proteins (May et al. 2007). The human *LRP4* is located at the cytogenetic band: 11p11.2, and at the genomic location: chr11: 46,856,717-46,918,650. *LRP4* was initially discovered in a study based on motif-trap screening method. The study group randomly selected long cDNA sequences (>5kb) and searched for genes encoding for proteins with multiple epidermal growth factor EGF-like motifs in human brain cDNA libraries, eventually they were able to identify novel proteins including the LRP4 protein (Nakayama et al. 1998).

LRP4 is also known as *MEGF7* (multiple EGF-like domain 7), it contains 38 exons and 1905 amino acid residues and is about 64 kb long. Its structure is composed of a ligand binding type repeat, EGF-precursor homology domains, a transmembrane domain, and a cytoplasmic tail. It has an NPxY sequence in its cytoplasmic domain, and a tetra-amino acid motif that mediates its coupling to the endocytic machinery (May et al. 2007). *LRP4* has most of its components at the extracellular domain (ECD) which has eight LDLα domains (class A repeats), four β-propeller domains (class B repeats), and a domain for O-linked oligosaccharide modification. The intracellular domain ICD only contains the NPxY motif and a PDZ-interacting motif at the C-terminus (Shen et al. 2015).

The function of *LRP4*, like the rest of LDL receptor family members, was first identified as an endocytic receptor that transports lipoproteins into cells by receptor-mediated endocytosis. In this

process, specific ligands are internalized after binding to their receptors on the cell surface then they will be moved to the endosome, and then to be discharged to other compartments inside the cell (Schneider and Nimpf 2003). However, after the identification of additional members of the LDL receptor family and studying their biology, it was revealed that these proteins not only function in lipid metabolism but also as direct signaling receptors for a broad range of cellular signaling pathways (May et al. 2007). For instance, Lrp4 antagonizes the activation of the canonical Wnt signaling (Johnson et al. 2005). One study showed that complete loss of Lrp4 function causes defects in the formation of multiple embryonic tissues in mice (Weatherbee et al. 2006). It was proved that Lrp4 is required for viability and for normal development of the lung, kidney and ectodermal organs (Weatherbee et al. 2006). In the same study, one of the most striking phenotypes caused by a lack of Lrp4 is paralysis at birth, which was proposed to be due to an early block in the development of the neuromuscular junction (NMJ) (Weatherbee et al. 2006). Similarly, *LRP4* mutations in humans are associated with several developmental defects, including kidney anomalies (Kariminejad et al. 2013), limb abnormalities (Li et al. 2010), cleft lip (Afzal et al. 2017), and even perinatal lethality (Lindy et al. 2014).

4.2 *LRP4* Gene Expression

LRP4 is expressed in various organs at different developmental stages (Figure 4.1). Yamaguchi et al. detected Lrp4 expression in mouse migratory primordial germ cells (PGCs) of the hindgut, in the spermatogonia of the neonatal and adult testes, and in the immature oocytes and follicular cells in females (Yamaguchi et al. 2006). However, Lrp4 cDNA was not detected in the blastocyst, embryonic stem cells and embryonic germ cells, which suggests Lrp4 is a molecular marker that distinguishes the germ cells from embryo-derived pluripotent stem cells (Yamaguchi et al. 2006).

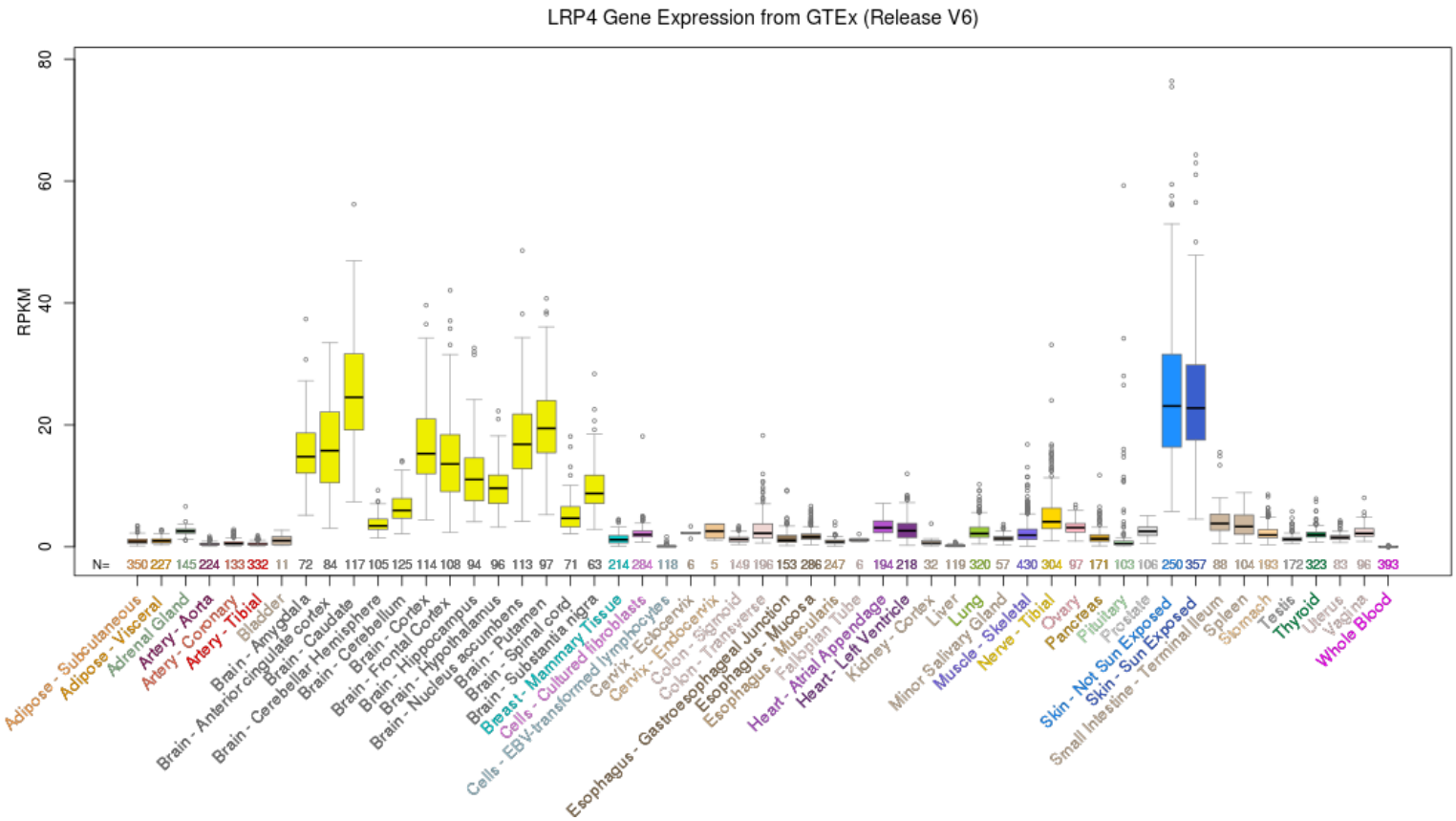

Figure 4.1: *LRP4* gene expression from GTEx. *LRP4* gene expression is differential in human normal tissues and organs. Available at https://gtexportal.org/.

A study carried out by (Weatherbee et al. 2006) showed that Lrp4 is strongly expressed in the proximal airways of the lungs as well as in the diaphragm. Newborn Lrp4-mutant mice showed respiratory defects, including a failure to expand the air passages in their lungs, which caused their early death (Weatherbee et al. 2006). Another study investigated *LRP4* expression in the developing kidney in both mouse and human (Karner et al. 2010). The authors revealed that *LRP4* is widely expressed in the kidney during development. In mice, complete absence of functional Lrp4 has led to unilateral or bilateral kidney agenesis (Figure 4.2) caused by a delay in the formation of an important component of the kidney called the ureteric bud. The ureteric bud is an epithelial tube that arises from the nephric duct and branches to give rise to the renal collecting

ducts system, and also promotes nephrogenesis (Karner et al. 2010). It is worth mentioning that *LRP4* renal expression is of great interest since many patients with Cenani-Lenz syndactyly present with renal abnormalities, ranging from complete agenesis to hypoplasia (Kariminejad et al. 2013; Steel et al. 2020).

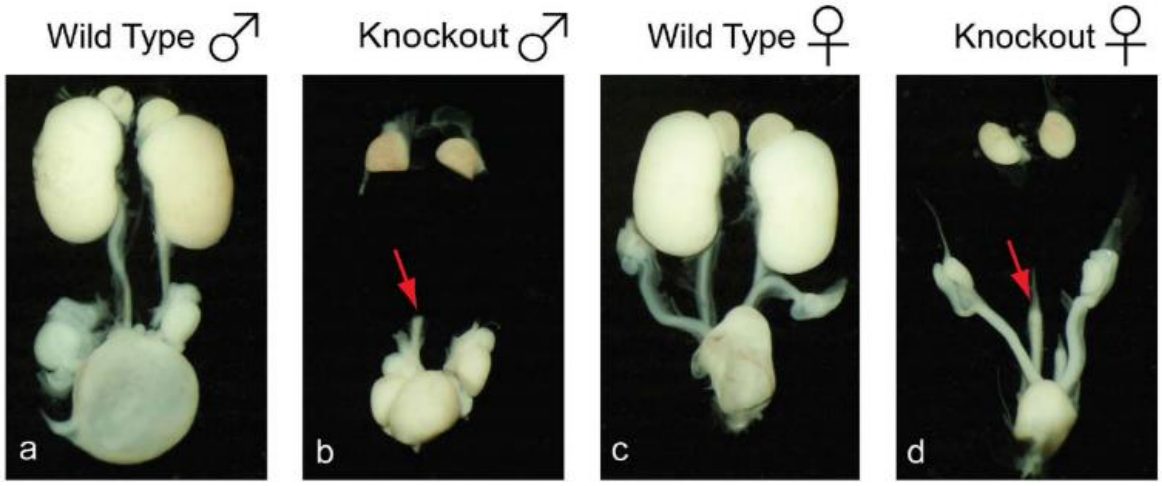

Figure 4.2: Kidney agenesis in Lrp4 knockout mice. Bilateral kidney agenesis in the Lrp4 knockout (b, d), compared to the wild type (a), with rudimentary ureters (red arrows). The lower urinary and genital systems of males and females remain intact, (Karner et al. 2010).

More importantly, LRP4 protein is present in human and rodent osteoblasts and osteocytes (Leupin et al. 2011). Choi and his colleagues showed that LRP4 regulates bone growth and turnover in vivo by directly binding two inhibitory regulators of the Wnt/ß-catenin pathway; one is sclerostin (SOST), an osteocyte secreted inhibitor of bone formation, and the second is Dickkopf 1 (Dkk1) which is required for embryonic head and limb development (Choi et al. 2009; Leupin et al. 2011).

Finally, another group reported that Lrp4 is expressed in epithelial cells during tooth development and that it binds a bone morphogenic protein (BMP) antagonist called Wise, through its highly conserved EGF-like domain and thus acting as a modulator of BMP and Wnt signaling during

tooth morphogenesis (Ohazama et al. 2010). Therefore, dental anomalies are often observed in Cenani-Lenz syndactyly affected individuals (Li et al. 2010).

4.3 *LRP4* Role in Cenani Lenz-Syndactyly

The first direct connection between *LRP4* and syndactyly was made in 2005, when a study group knocked out the gene activity in mice by homologous recombination in embryonic stem cells, and noted polysyndactyly (a phenotype that is characterized by the fusion and duplication of digits of the fore and hind limbs) in homozygous Lrp4 deficient mice (Johnson et al. 2005). The authors demonstrated that the loss of Lrp4 function results in an abnormal expression of important signaling molecules like Fgf8, Shh, Bmp2, Bmp4 and Wnt7a, which are crucial for normal digit formation (Figure 4.3). They further reported that the phenotype was often combined with mild craniofacial and tooth development abnormalities, which remarkably resemble the clinical features of Cenani-Lenz syndactyly syndrome in humans (Johnson et al. 2005). More interestingly, LRP4 gene has also been found to be linked to syndactyly in cattle (Duchesne et al. 2006; Drögemüller et al. 2007), Drögemüller et al. studied sixteen animals from different breeds affected by congenital syndactyly (Figure 4.4) and identified four novel missense mutations in LRP4 gene (Drögemüller et al. 2007).

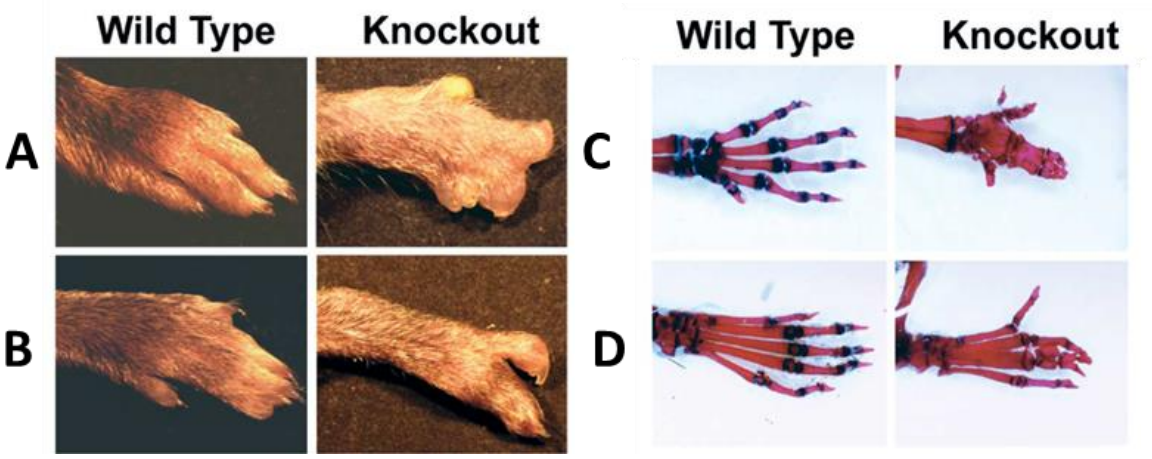

Figure 4.3: Polysyndactyly in Lrp4-knockout mice. (A) Forelimbs and **(B)** hindlimbs of wild type and knockout adult mice. Duplication and fusion of digits are apparent in the mutants. **(C)** Alcian Blue and Alizarin Red staining of the autopod of wild type and knockout forelimbs and **(D)** hindlimbs. Alcian Blue stains cartilage and Alizarin Red stains bone, (Johnson et al. 2005).

Li and his colleagues studied all the reported CLS cases, and were the first who mapped Cenani-Lenz syndactlyly locus, and identified loss of function mutations in *LRP4* gene. Of the study group, only two families did not exhibit *LRP4* mutations (Li et al. 2010). Moreover, the authors demonstrate that Lrp4 is able to inhibit the Wnt-induced activation of the Luciferase reporter in an activity assay, assuming that Lrp4 antagonizes the Lrp5/6 mediated activation of the pathway (Li et al. 2010). One study has also shown that LRP4 binds to sclerostin and enhances its suppressive effects on the canonical Wnt signaling pathway (Leupin et al. 2011)

Figure 4.4: Congenital syndactyly in cattle. Italian Holstein calf with two variably affected syndactylous forefeet, (Drögemüller et al. 2007).

In summary, LRP4 is a strong suppressor of Wnt signaling, and hence, loss-of-function mutations of *LRP4* will lead to Wnt signaling over-activation. Excessive Wnt signaling causes β-catenin accumulation, which in turn upregulates fibroblast growth factor 8 levels in the apical ectodermal ridge AER. This results in suppression of retinoic acid in the mesoderm. Prolonged inhibitory effect on retinoic acid will reduce apoptosis in the spaces between the digits, leading to their fusion (Al-Qattan 2014).

4.4 Mutational Spectrum of *LRP4*

Most CLS affected individuals have been described with missense and splice mutations in *LRP4* (Li et al. 2010). One individual has been described with a homozygous nonsense mutation (Kariminejad et al. 2013). A more severe case of CLS was reported by Lindy and her colleagues who presented two sibling fetuses with a prenatal lethal form of CLS including severe renal anomalies, resulting from compound heterozygosity for two novel truncating mutations in *LRP4*. The fetuses showed mesomelic limb reductions, oligosyndactyly, and genitourinary malformation (Figure 4.5) (Lindy et al. 2014).

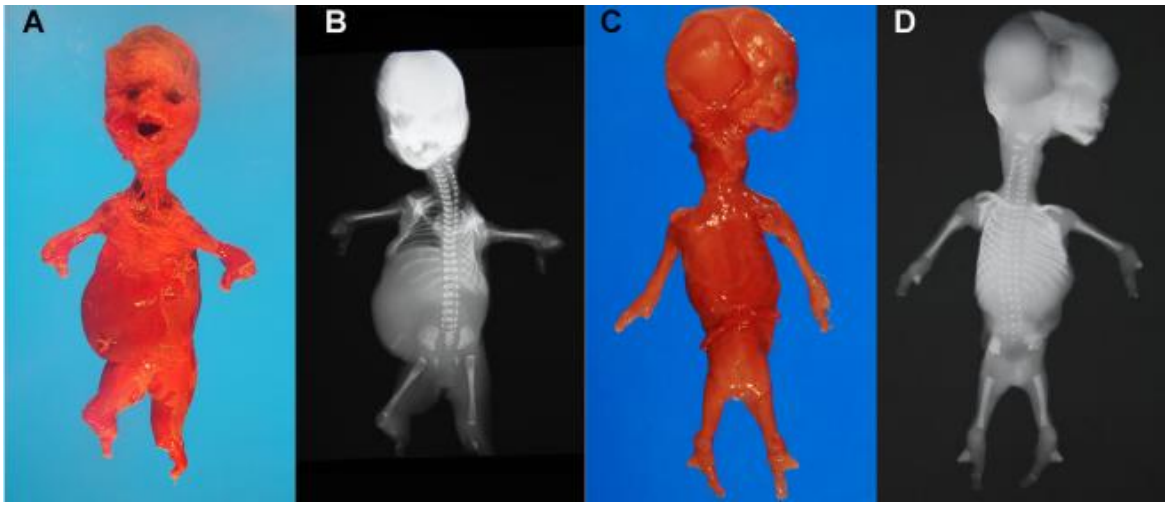

Figure 4.5: Postmortem radiograph of the sibling fetuses reported by Lindy et al. A and **C**: Photographic images of the fetuses. **B**: Radiograph of the first fetus, showing the ossification centers in the

micromelic segments and four-limb oligosyndactyly. **D**: Radiograph of the second fetus, showing wide ribs, wedge-shaped bony protuberance from the middle segments and four-limb oligodactyly with ossification of two to four rays in the hands and feet (Lindy et al. 2014).

Other severe phenotypes with additional features such as hearing loss, high arched palate, cleft-lip, enamel hypoplasia, supernumerary nipples short stature, and hypoplastic shoulder joint have been reported (Kariminejad et al. 2013; Afzal et al. 2017). On the mild end of the spectrum, homozygosity for the missense variant, p.L953P, in *LRP4* was found in a large family with a mild CLS phenotype restricted mainly to the upper limbs and kidneys (Khan et al. 2013). Lower limb malformations were either mild or absent and there were no radioulnar synostosis or craniofacial involvement.

LRP4 appears to control bone density in humans. *LRP4* polymorphisms are associated with altered bone mineral density and lower fracture incidence in genome-wide association studies (Monroe et al. 2012; Maeda et al. 2019). In addition, two mutations (R1170W and W1186S) in the extracellular region of *LRP4* were found in patients exhibiting bone overgrowth (Leupin et al. 2011). These amino acid substitutions impaired LRP4 association with Sclerostin (Scl), an inhibitor of bone formation. (Bullock et al. 2019).

Recently a research group has reported a patient, in whom they found a novel homozygous splice-site variant c.1048+6T>C in *LRP4* using whole exome sequencing. The patient was initially misdiagnosed with isolated CLSS-like or Malik-Percin-like syndactyly but he turned out to have sclerosteosis type 2 (SOST2) (Bukowska-Olech et al. 2020). Another study has reported two novel variants p.D1403H and p.Q1564K, which are located within the fourth β-propeller of the extracellular protein domain of LRP4, that are associated with isolated syndactyly (Figure 4.6) (Sukenik Halevy et al. 2018).

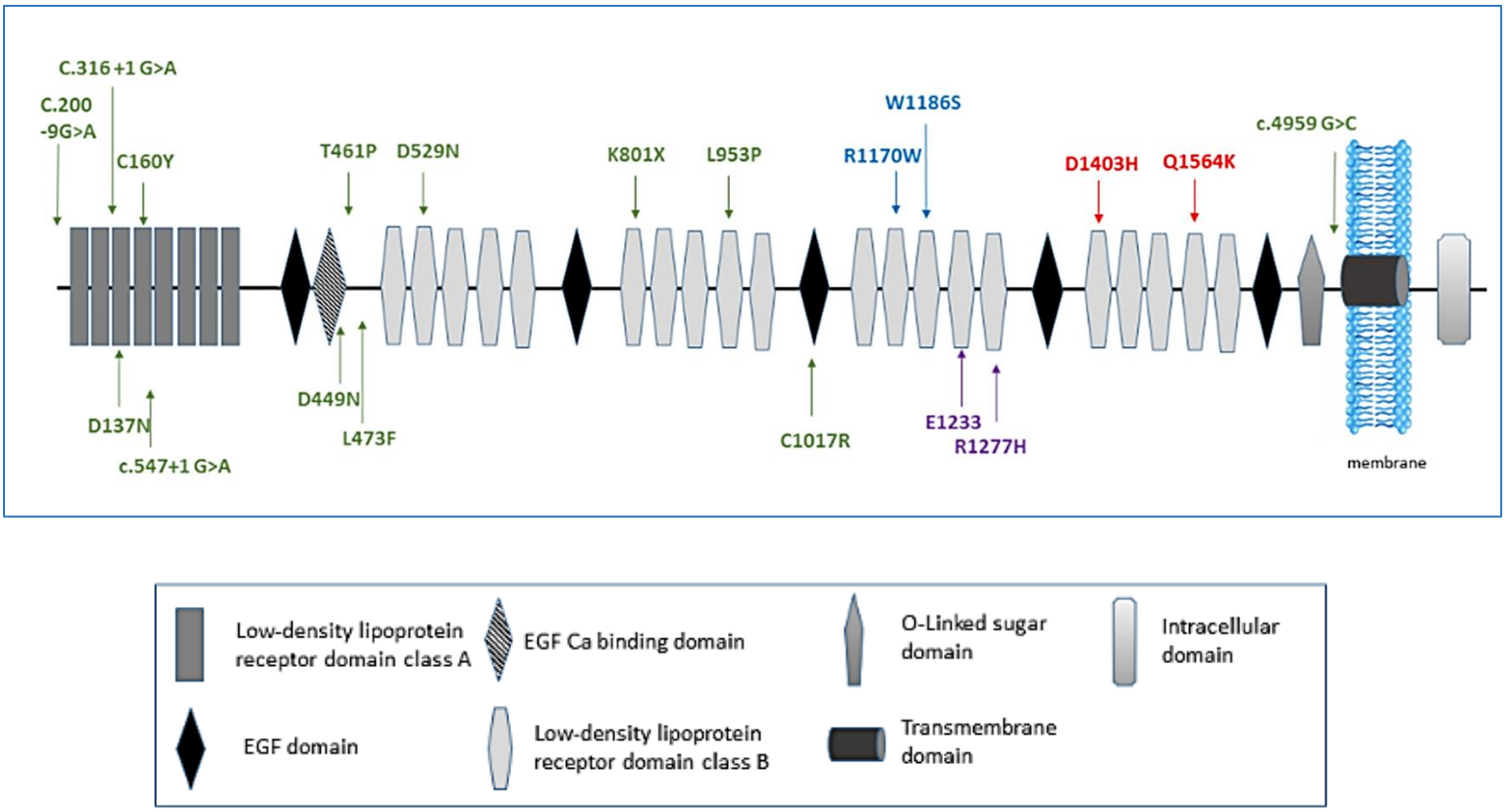

Figure 4.6: Position of all published pathogenic variants in *LRP4*.

CHAPTER 5

Materials and Methods

5.1 Ascertainment of Study Subjects

A large Palestinian family with multiple individuals affected with different conditions has been enrolled in the study. Within the same family, some members presented with limb malformation, others with intellectual disability and one with cleft lip. Our research staff has first met the family on one of our periodic visits to The Palestinian European Fertility Center, while we were recruiting families to participate in an ongoing lab project studying male infertility. The family was further contacted and they seemed to have congenital limb deformity but without a clear diagnosis yet. All subjects or their legal representatives, who agreed to participate in the study, gave written informed consent according to the protocols approved by the Bethlehem University Research Committee. After arranging with the family, subjects were directly interviewed at their households to ensure their collaboration and for their own convenience. In those who were dead, younger than 12 years, or otherwise unavailable, we interviewed the relative deemed to be the best informant regarding the subject's history. All the affected members were asked to provide us with any medical report related to their condition. Blood samples were collected from all available participants by our lab staff members, who have valid profession-practicing license and certified to draw blood by the Palestinian Ministry of Health. The affected family members were photographed after their permission, and were offered to have X-ray imaging and also a visit to Pal-Orthopedics Center, for further assessment by orthopedists and physicians.

5.2 Genomic DNA Extraction from Blood by Salting-out Method

A total of sixteen blood samples were collected into EDTA vacutainer tubes. For each sample, 5-10 ml of whole-blood was placed in a 50-ml conical tube. Around 40 ml of pre-chilled RBC lysis buffer (155 mM NH_4CL, 100 M NH_4HCO_3, 0.1 mM EDTA) was then added. The tubes were incubated on ice for 30 minutes and inverted occasionally, then centrifuged at 2000 rpm for 10 minutes at 4^oC. The supernatant was discarded without disturbing the pellet. To wash the pellet, 15 ml of RBC lysis buffer was added, tubes were briefly vortexed then centrifuged again at the same conditions. After discarding the supernatant, the remaining moisture was removed by inverting the tube and blotting it onto tissue paper. To the white pellet, 3 ml of DNA lysis buffer (50 mM Tris HCL pH = 7.5, 100 mM NaCl, 1 mM EDTA), 100 µl of sodium dodecyl sulfate SDS (Amresco, Cat# 1328-M112) and 100 µl of 5mg/ml Proteinase K (Amresco, Cat# E195) were added. The pellet was resuspened by vortexing, and the tubes were incubated overnight at 37^oC with shaking. After the digestion is completed, 1 ml of 6M NaCl was added and the tubes were vigorously vortexed then centrifuged at 3000 rpm for 20 min at 25^oC. Only the supernatant was transferred to a new set of 15-ml tubes. Pre-chilled 100% absolute ethanol was added to each tube, double the volume of the supernatant. The tubes were gently inverted 5-6 times to allow the DNA to precipitate. Using a freshly prepared flamed Pasteur pipette the white DNA threads were spooled onto the hooked end. DNA was washed in 70% ethanol, and allowed to air-dry briefly. DNA was finally transferred to a 1.5-ml screw cap tube, and dissolved in 200-600 µl of 0.02% Sodium azide (Sigma Aldrich, Cat# S2002).

5.3 Genotyping

5.3.1 Primer Design

The primer sequences used in this thesis are listed in Appendix I, Table 10.1. All primers were designed using Primer3 Input (version 4.0.0) software (http://primer3.ut.ee). In-silico PCR was done on all primer pairs using UCSC In-Silico PCR online tool (https://genome.ucsc.edu/cgi-bin/hgPcr). The primers annealing temperatures were calculated based on Promega T_m Calculator (https://worldwide.promega.com/resources), which takes into account the GoTaq buffer composition not only the GC content of the primers.

5.3.2 Polymerase Chain Reaction

To carry out a PCR reaction, DNA polymerase, template DNA, forward and reverse primers, dNTPs, $MgCl_2$, PCR buffer and sterile water are needed. For a total volume of 25 ul for one PCR reaction, 12.5 ul of GoTaq Green Master Mix (Promega, Cat# M7122), which contains GoTaq DNA Polymerase, dNTPs, $MgCl_2$ and buffer, was added to 10.5 ul of nuclease-free water and 0.5 ul of each forward and reverse primers. In a clean area and on ice, a master mix containing the reagents, excluding the DNA template was prepared. Each volume was multiplied by the number of intended reactions. A no template control (NTC) was included within each mix to exclude any nucleic acid contamination. 24 ul of the master mix was pipetted in each reaction well, followed by the addition of 1 ul of the DNA template (50-100 ng). The PCR reactions were carried out in the thermocycler GeneAmp^{TM} PCR system 9700 (Applied Biosystems) using the following program. An initial denaturation at 94°C for 3 min, followed by a 35 cycles of a denaturation step at 94°C for 3 min, an annealing step at 60°C for 30 sec, and an extension step at 72°C for 30 sec. Afterwards, a final extension at 72°C for 3 min, and finishing with a hold at 4ºC.

5.3.3 Gel Electrophoresis of Amplified PCR products

1.5% agarose gel was prepared by mixing agarose powder with 100 mL 1X TAE buffer (2 M Tris pH= 8, 1 M acetic acid, 0.05 M EDTA pH = 8) in a microwavable flask. The flask was microwaved for 2 min with occasional swirling until the agarose was completely dissolved. The agarose solution was allowed to cool down for about 5 min, and then Ethidium Bromide (EtBr) (Amresco, Cat# E406-5ML) was added to a final concentration of approximately 0.2-0.5 µg/mL. The agarose was poured into a gel tray with the well comb in place and let at room temperature for 20-30 min. Once solidified, the agarose gel was transferred into the gel box and covered with 1X TAE buffer. A molecular weight ladder (GeneRuler, Thermo Scientific, Cat# SM0241) was loaded into the first lane of the gel followed by 5 ul of each PCR product to the additional wells. There was no need to add a loading dye to the PCR products since the GoTaq mix contains two dyes (blue and yellow) that allow monitoring of progress during electrophoresis. The blue dye migrates at the same rate as 3–5kb DNA fragments. The yellow dye migrates ahead of primers (<50bp). Electrophoresis was performed at 100 V for 40 minutes. Molecular Imager, Gel DOC™ XR+ Imaging System, BioRAD was used for DNA visualization under UV light.

5.3.4 Purification of PCR product

To remove excess primers and unincorporated nucleotides, PCR products were enzymatically cleaned using ExoSAP-IT™ PCR Product Cleanup Reagent (Cat# 78200.200.UL, Applied Biosystems), which is a mixture of exonuclease I combined with shrimp alkaline phosphatase (SAP). Exonuclease I removes residual single-stranded primers and any single-stranded DNA produced during PCR. SAP removes the remaining dNTPs from the PCR mixture. 2ul of ExoSAP solution was directly added to 5 ul of each PCR product. The reaction has taken place in

thermocycler starting at 37° C for 30 min, to digest excess primer and dephosphorylate the nucleotides, followed by a second incubation step at 80° C for 15 min, to inactivate the enzymes. The reaction was held at 4° C, and the products were stored at -20° C until use.

5.3.5 Sanger Sequencing

5.3.5.1 Sequencing of the Purified PCR Product

For each sequencing reaction, 1 ul of Big Dye Terminator v1. Cycle Sequencing (Applied Biosystems, Cat# 4336768), 3.5 ul of 5X buffer (Applied Biosystems, Cat# 4336697), 2 ul of 5uM primer (forward or reverse) were mixed with 11.5 ul molecular grade water and 2 ul of the clean PCR product. The reagents needed for each sequencing reaction are listed in Table 5.1, and the sequencing reactions were carried out in the thermocycler using the program showed in Figure 5.1.

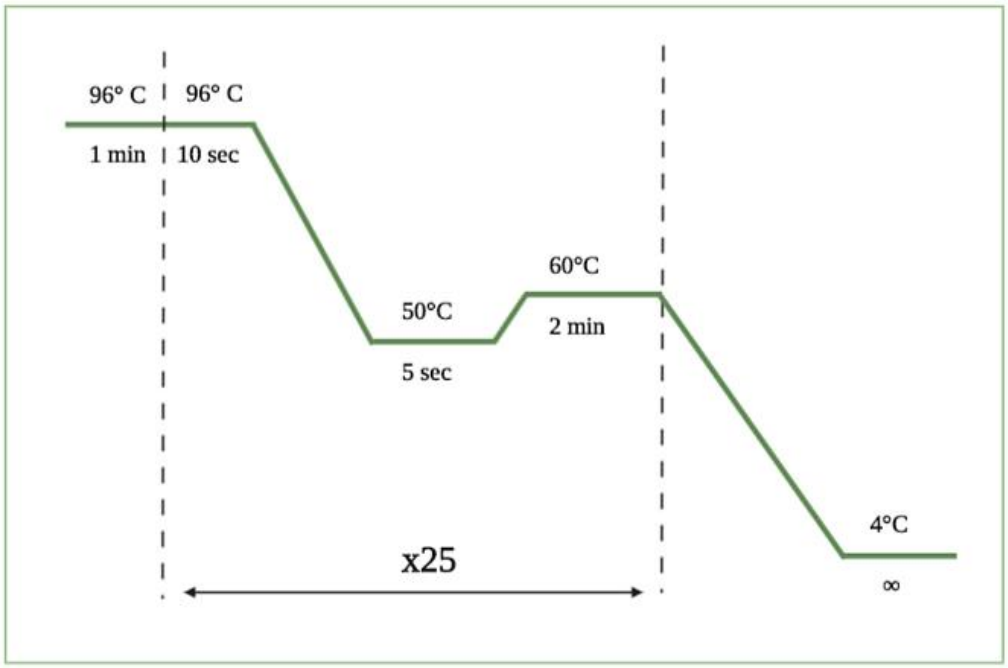

Figure 5.1: The Thermal cycler program for sequencing reaction.

Table 5.1: Reagents needed for sequencing reaction

	Final Concentration in Reaction	1X Reaction
Big Dye Buffer	5X	3.5
Big Dye Terminator	2.5X	1
Forward/Reverse Primer	5 pmole/ul	2
DNA Template	3-10 ng	2
D.W 20 ul-total		11.5

5.3.5.2 Cleaning of the Sequenced PCR Product and Capillary Electrophoresis

5 ul of freshly prepared 125 mM EDTA was added to each sequenced PCR reaction and mixed well by continuous pipetting. 60 ul of 100% pre-chilled ethanol was then added. The plate was sealed with self-adhesive film and vortexed for 2 min, then centrifuged at 2000-3000X g for 30 min at 4^{o}C. The plate was removed and flipped upside down on a tissue paper and centrifuged flipped for 1 min at 100X g. 60 ul of 80% cold ethanol was added. The plate was sealed, vortexed and centrifuged again at 1650X g for 15 min at 4^{o}C. The plate was inverted again on a tissue paper and centrifuged for 1 min at 100X g. The plate was then incubated in the dark at room temperature for 15 minutes. 10 ul of HiDi Formamide (Applied Biosystems, Cat# 4311320) was added to each well. The plate was incubated on a hot plate at 95^{o}C for 3 min to denature the DNA then put on ice for another 3 min. The samples were loaded and capillary electrophoresis was performed on ABI 3130 Genetic Analyzer (Applied Biosystems, S/N:20355-023) to start the run.

5.3.6 Analysis of Sequencing Data

The sequence files were analyzed using SnapGene software (https://www.snapgene.com/snap gene-viewer/). The sequences were aligned against the web-based human reference genome

(UCSC, Human GRCh37/hg19). The identified variants were tested for their potential effect of pathogenicity via SIFT (https://sift.bii.a-star.edu.sg/), Polyphen (http://genetics.bwh.harvard .edu/pph2/) and MutationTaster software (http://www.mutationtaster.org/). The UniProtKB database was used for obtaining the sequence and functions of various domains of the LRP4 protein (https://www.uniprot.org/uniprot/O75096). Multiple alignment of the variant was done using the online tool MUSCLE.

5.4 Next Generation Sequencing

Next generation sequencing was performed at The Institute of Human Genetics, University of Göttingen, Germany. The TruSight One Sequencing Panel (Illumina) was used for sequencing the whole gene regions of 4813 disease-associated genes. In accordance with the kit protocol; genomic DNA tagmentation, cleaning up of the tagmented DNA, cleaning up of the accumulated DNA, hybridization of the probes, catching the hybridized probes, second hybridization, second catch, cleaning up of the catched library, accumulation of the enriched library, cleaning up of the accumulated enriched library were performed. The Enrichment of the 50 ng DNA was done using the TruSight One chemistry (version 1). The generated library was sequenced on MiSeq sequencer (Illumina) with 10x minimum depth of coverage at more than 95% of targets. The variant was analyzed via the CCG varbank (https://varbank.ccg.uni-koeln.de/). In order to confirm the pathogenic variant identified by NGS, bidirectional Sanger sequencing was performed.

CHAPTER 6

Results

6.1 Clinical Presentation of CLS-Family

The family members originated from Yatta town, south of Hebron, West Bank. A detailed family pedigree is illustrated in Figure 6.1. Five individuals were examined and diagnosed with Cenani-Lenz syndactyly. Diagnosis was confirmed by Dr. Bernd Wollnik, MD, Germany, with the help of clinical manifestations and X-ray imaging. Of the affected individuals, a 6-year-old boy (IV-4) and his 5-year-old brother (IV-3), were born after a normal pregnancy and delivery. The two are the only children of first-cousin healthy parents. Their unusual face and limbs were noted at birth. Subsequent motor development was impaired by the limb anomalies but cognition appeared normal. Clinical examination of the older brother (IV-4) showed extensive limb malformations of both hands with a prominent forehead, downslanting palpebral fissures, sparse eyebrows and eyelashes, and large, prominent ears (Figure 6.2). Radiological examination of his upper limbs revealed bilateral malformation and irregular synostosis of the phalanges, metacarpals and carpals (Figure 6.3) compared to the normal hand X-ray. The second child (IV-3) also showed severe involvement of both hands. He further exhibited oro-facial symptoms like broad forehead, high hairline, depressed nasal bridge and cleft-lip (Figure 6.2). His radiographs showed complete disorganization of all bones of hand to such an extent that some phalangeal elements are not identifiable. Reduction of the digital rays, fusions and hypoplasia/aplasia of carpals, metacarpals and phalanges were also present, as well as fusion in the radius and ulna bones in his right hand (Figure 6.4). In the feet of both children (IV-3, IV-4), the only abnormality was partial soft tissue syndactyly between the second and third toes.

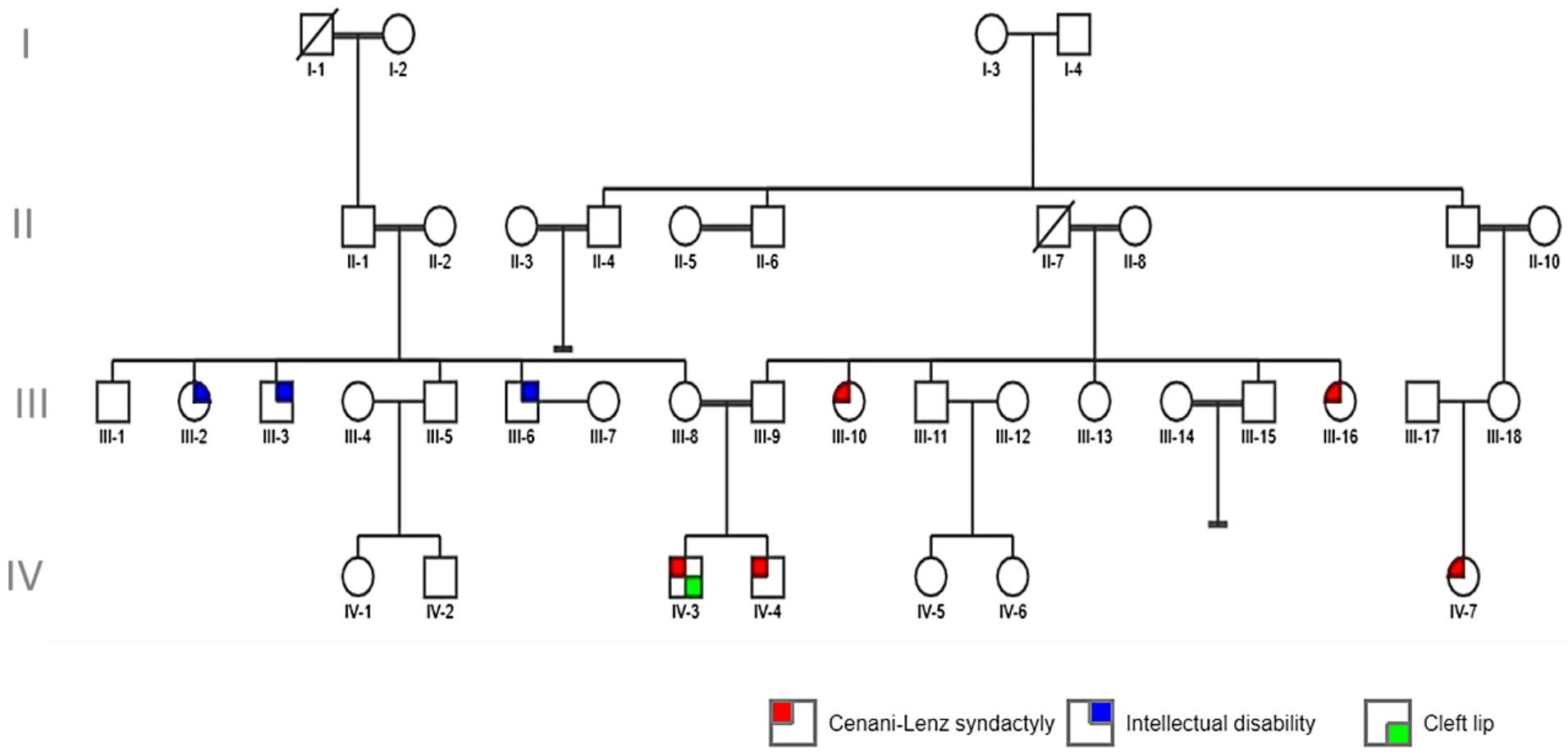

Figure 6.1: Pedigree of Cenani-Lenz syndactyly family, showing affection status of sampled individuals. Of the family members, five individuals presented with syndactyly and one with cleft lip, others have intellectual disability that is not fully characterized.

Figure 6.2: Facial features of two CLS-patients (IV-3 and IV-4). Individual IV-4 has a prominent forehead, downslanting palpebral fissures, sparse eyebrows and eyelashes, and large, prominent ears. Individual IV-3 shows broad forehead, high hairline, depressed nasal bridge and cleft-lip.

The phenotypic variability was high among affected individuals of the family. The other affected family members are two sisters (III-16 and III-10) with ages 34 and 16 years, respectively. Their clinical examination showed asymmetrical syndactyly accompanied by shortening in the forearms and absence of some digital rays (Figure 6.5). Unfortunately, their radiographs are not available therefore, other abnormalities, including radioulnar synostosis, radius head dislocation, shortening of radius/ulna, cannot be excluded. The affected subjects had normal vision, hearing and speech but were unable to lift heavy objects. The lower extremities were generally less severely affected.

Figure 6.3: Radiographic and clinical manifestations for patient IV-4. Radiographs of the right and left hands show bilateral malformation and irregular synostosis of the phalanges, metacarpals and carpals

Figure 6.4: Radiographic and clinical manifestations for patient IV-3. Radiographs show complete disorganization of all bones of hand, reduction of the digital rays, fusions and hypoplasia/aplasia of carpals, metacarpals and phalanges as well as fusion in the radius and ulna bones in his right hand.

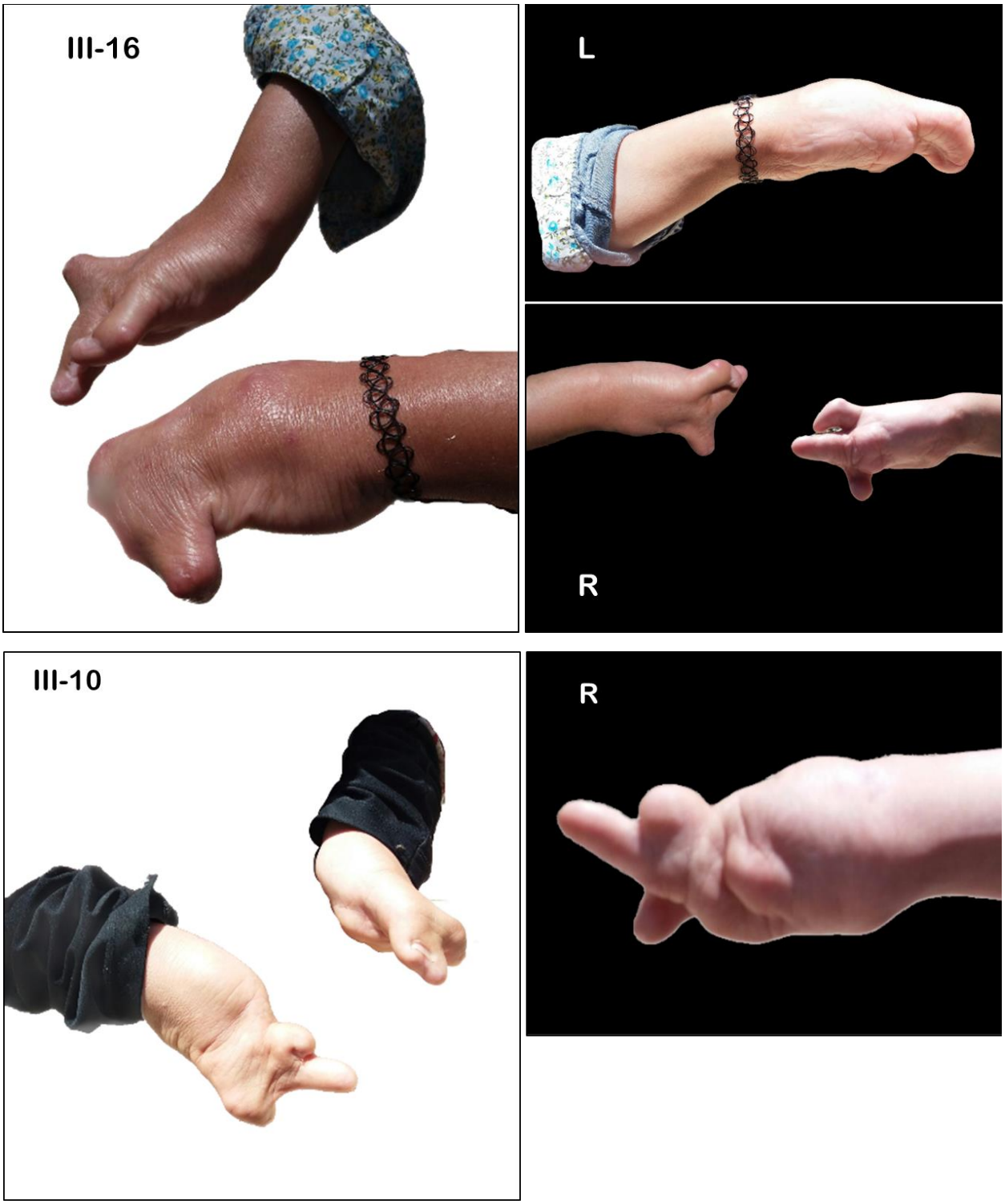

Figure 6.5: Hand anomalies of the patients III-16 and III-10. Images show dorsal and palmar views of the left and right hands. Single unilateral metacarpal synostosis, one partial syndactyly and duplication of one phalangeal ray

6.2 Genetic Analysis

6.2.1 Excluding Known *LRP4* Allele in Jordanian Population

As an initial work-up, all sampled affected individuals were first tested for the previously reported *LRP4* mutation that was identified in one Jordanian patient in exon 11 (c.1382A>C, p.T461P), using the primers listed in Appendix I (Table 10.1). Sequence analysis showed that none of the affected individuals had this mutation, and none of the parents carries this mutation in the heterozygous state.

6.2.2 Next-Generation Sequencing Analysis Results

Sequence analysis of the disease-associated panel on DNA of the patients (IV-3, IV-4) identified the homozygous missense mutation c.3049T>C in exon 22 of the *LRP4* gene. Both parents, III-8 (mother) and III-9 (father), carry the mutation c.3049T>C in the *LRP4* gene in the heterozygous state. At the protein level, this mutation leads to the substitution of a cysteine at the amino acid position 1017 by arginine (p.Cys1017Arg).

6.2.3 Candidate Variant Validation by Sanger Sequencing

The target gDNA position and flanking sequences 471 bp were amplified in all available family members using the primers listed in Appendix I (Table 10.1). The PCR products were then sequenced in both directions. Segregation analysis confirmed that the *LRP4*_ p.Cys1017Arg variant was present in all affected individuals (III-10, III-16, IV-3, and IV-4) in the homozygous state. Except for one affected individual that was not available for testing (IV-7). Sanger sequencing results of the sampled members, 4 affected and 12 unaffected individuals, showed that this mutation segregates in a recessive mode of inheritance. It also revealed that the unaffected parents were heterozygous for the variant and the affected members were homozygous, while the

unaffected siblings were wild type or heterozygous for the mutation. In the mutant sequence, the homozygous shows a nucleotide C instead of T that appeared in the wild type as in Figure 6.6, that shows the chromatograms of the parents and an affected child as compared to the wild type.

Homozygous Child (Affected) IV-4

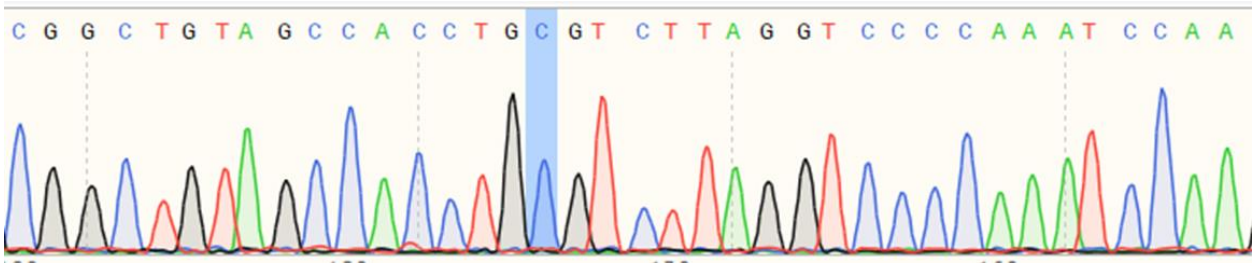

Hetrozygous Father (Unaffected) III-9

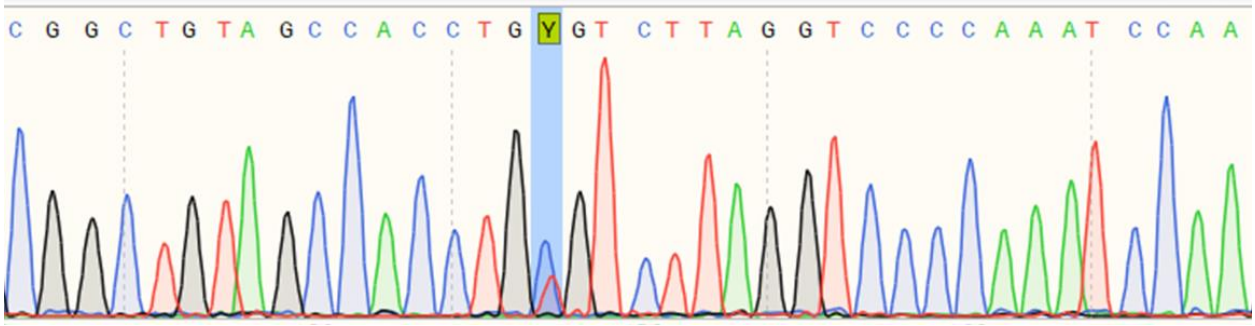

Wild-Type Sequence

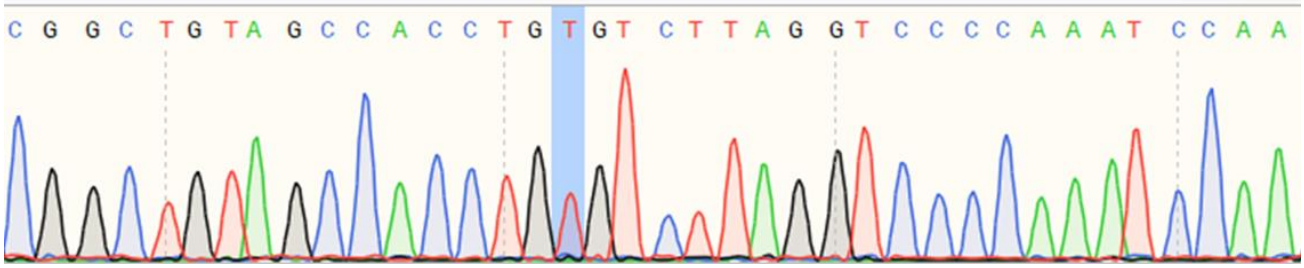

Figure 6.6: **Chromatograms for some of the family members.** Homozygous mutant sequence showing the nucleotide C instead of T, while it appears in the carrier state in heterozygous unaffected individuals compared to the wild-type sequence.

6.2.4 Sanger Sequencing of Candidate Variant in *LRP4* in Palestinian Controls

Population specific controls were around 100 healthy unrelated Palestinians from different areas of Palestine. Further to confirm the pathogenicity of the mutation, controls were sequenced for the *LRP4*_p.C1017R variant. The alteration was not present in any of the healthy controls neither as homozygous or heterozygous.

6.3 *In silico* predictions and protein analysis

The pathogenicity analysis was performed using the web-based tools; MutationTaster (http://www.mutationtaster.org/) PolyPhen-2 (http://genetics.bwh.harvard.edu/pph2/) and SIFT (http://sift.jcvi.org/). The identified variant is predicted to be "pathogenic" and "disease causing".

6.3.1 Conservation and Alignment

LRP4 protein sequences from multiple species were aligned using the online multiple sequence alignment tool MUSCLE (https://www.ebi.ac.uk/Tools/msa/muscle/) (Figure 6.3). Accession numbers used for the alignment: Homo sapiens (O75096), Bos taurus (Q00KA9), Canis familiaris (J9P7Q4), Mus musculus (Q8VI56), Rattus norvegicus (Q9QYP1) Pan troglodytes (H2Q3I3), all are available at UniProtKB database (https://www.uniprot.org/). Results were viewed by Jalview software (Waterhouse et al. 2009), and it showed that cysteine residues are highly conserved.

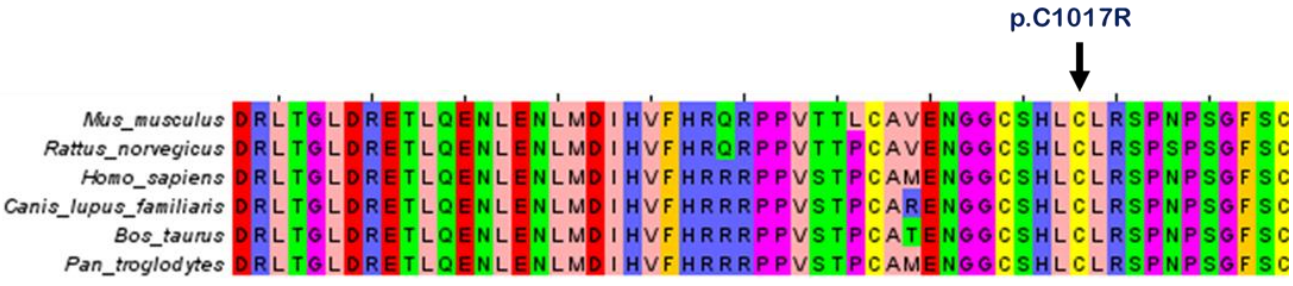

Figure 6.7 Multispecies protein sequence alignment of parts of LRP4. The cysteine residues in the EGF domain are highly conserved among different species. The identified mutation is indicated by arrow.

CHAPTER 7

Discussion

The aim of this project was to identify the underlying molecular cause of Cenani-Lenz syndactyly in a Palestinian family diagnosed with this unique, rare and heterogeneous phenotype. Owing to the fact that Cenani-Lenz syndactyly has not been reported among the Palestinian population before, it was quite challenging to reach a final diagnosis of the patients. Another diagnostic challenge was the high phenotypic variability among affected individuals of this family, as well as between the limbs of the same affected individual. Most of the affected family members showed asymmetrical, bilateral, complete and/or partial syndactyly of the upper and lower limbs. Lower limbs deformations were mild, whereas the upper limbs were severely affected. In order to obtain diagnostic certainty, and a clinically well-defined genetic condition, the need has emerged for molecular testing. By applying a combination of different strategies including Next-generation sequencing (NGS), Sanger sequencing and bioinformatics tools, we were able to identify a missense *LRP4* mutation that has a major contribution to CLS observed in this family.

The *LRP4* gene encodes a lipoprotein receptor known for its regulatory effects on Wnt signaling, a pathway that plays a pivotal role in limb development. The variant p.Cys1017Arg was detected in a homozygous state in the affected individuals, while heterozygous in the parents, and it was not found after being further screened in at least 100 healthy control individuals. The identified mutation has been previously reported in a large CLS family from Pakistan with six affected family members (Li et al. 2010). This missense substitution is located in the fourth EGF-like calcium-binding domain of the LRP4 protein. There are six epidermal growth factor EGF domains in LRP4, which are believed to contribute to membrane binding and secretion of the protein. Each EGF

domain contains six cysteine residues that are required for the formation of disulfide bonds (Figure 4.6). However, this mutation (p.Cys1017Arg) is predicted to result in loss of one of the six cysteine residues. The cysteine at amino acid 1017 is found to be highly conserved among various species. The evolutionary conservation emphasizes the importance of Cys1017 in its EGF-like domain (Figure 6.6).

Unfortunately, there are no functional studies on this mutation yet. However, a recent study has reported a similar mutation (p.R373W) in the first EGF-like domain in a Jordanian patient (Tian et al. 2019). They performed a functional test called TOP-Flash luciferase assay to analyze the effect of R373W mutation on the activation of canonical Wnt signaling, in which they transfected HEK293T cells with wild-type and mutant *Lrp4* plasmids, together with *Lrp6* and *Wnt* plasmids, then measured the luciferase activity. They showed that the R373W mutation has abolished the antagonistic LRP4 effect on LRP6-mediated activation of Wnt/β-catenin signaling (Figure 7.1), which could be due to the failure of the mutant LRP4 protein to be efficiently transported to the plasma membrane (Tian et al. 2019). Thus, we assume that our mutation (p.Cys1017Arg) has the same proposed mechanism of pathogenesis that may have led to the phenotype altering the normal Wnt signaling pathway in our patients.

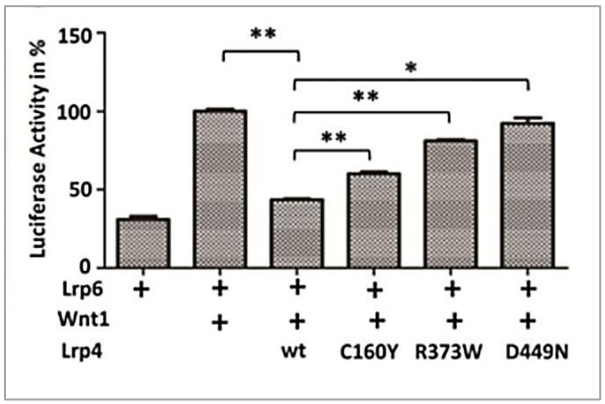

Figure 7.1: The effect of R373W mutation in LRP4 on the Wnt signaling in vitro. TOP-Flash luciferase assay was performed to quantify the Wnt activity in HEK293T cells co-transfected with *Lrp6*, *Wnt1*, wild-type and mutated *Lrp4* plasmids. *Wnt1* was able to significantly activate the *Lrp6*-mediated β-catenin signaling. Additional co-expression of *Lrp4* potently antagonized this activation. In contrast, co-expression of the missense mutation abolished the observed antagonistic *Lrp4* effect on *Lrp6*-mediated activation of Wnt/ β -catenin signaling (Tian et al. 2019).

CHAPTER 8

Conclusion

In this thesis, we report the first Palestinian family diagnosed with Cenani-Lenz syndactyly. The approach employed here involved family ascertainment and extensive detailed phenotyping by multiple physicians and orthopedists, as well as investigation of candidate causative genes using targeted next-generation sequencing and further validation and segregation analysis by Sanger sequencing.

The results revealed the missense alteration (p.Cys1017Arg) in *LRP4* gene, which is proposed to abolish the inhibitory effect of *LRP4* and thus will lead to over activation of the Wnt pathway. These cases further contribute to the phenotypic spectrum seen in Cenani-Lenz syndactyly, and support earlier reports of genotype–phenotype correlations.

This project will also contribute to the understanding of the pathogenesis underlying Cenani-Lenz syndactyly, improving clinical and molecular diagnosis; thus, making genetic counseling and prenatal testing easier in future. With the advances in preimplantation genetic diagnosis and other advanced reproductive techniques, and with the discovery and expansion of our knowledge about various genetic conditions, more opportunity is made for the families. Families can be given more detailed and specific information, and informed choices about how to proceed in preconceptional and prenatal genetic counseling.

In addition, because the key genes that control limb formation are also involved in many other developmental contexts, the knowledge gained from such studies of the limb can be applied to understanding the development of other tissues and organs.

Future Perspectives

To further validate the pathogenicity of our identified variant (p.C1017R), we propose to functionally study the effect of mutated LRP4 on the Wnt pathway activity. One approach is to measure the accumulation of β-catenin in the nucleus after transfecting the Wild-type and mutant LRP4 plasmids in HEK293T cells. β-catenin can be detected either by immunofluorescence or by doing extraction of nuclear and cytoplasmic fractions and check if β-catenin levels increase in the nuclear fraction when the Wnt is activated. Another approach is to measure the expression of β-catenin downstream target genes such as LEF/TCF in the presence of Wild-type and mutant LRP4.

As a start, we contacted Dr. Inga Koneczny (Medical University of Vienna, Vienna, Austria) who kindly provided LRP4-GFP plasmid (Origene RG217609) (Figure 8.1) that was created by Prof. Socrates Tzartos (Hellenic Pasteur Institute, Athens, Greece). We are planning to insert our variant by site directed mutagenesis then proceed with the transfection and expression analysis.

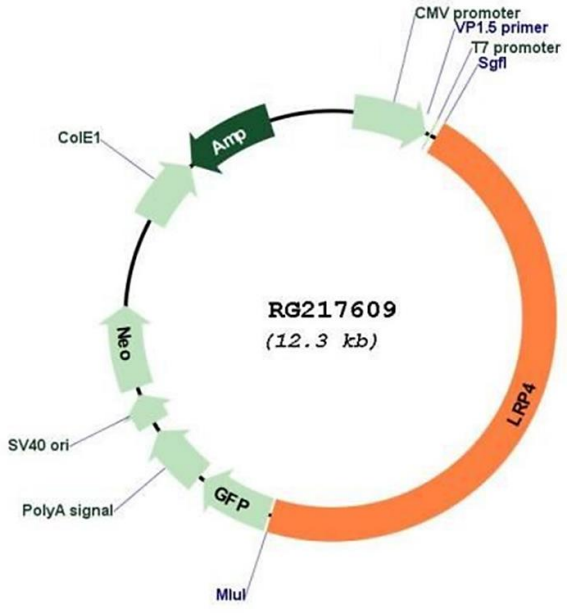

Figure 8:1: Plasmid map for human LRP4-GFP (Origene RG217609)

CHAPTER 9

References

Abu-Libdeh, B. and Teebi, A.S. 2010. Genetic Disorders Among the Palestinians. In: Teebi, A. S. ed. *Genetic Disorders Among Arab Populations*. Berlin, Heidelberg: Springer Berlin Heidelberg, pp. 491–514.

Afzal, M. et al. 2017. Novel splice mutation in LRP4 causes severe type of Cenani-Lenz syndactyly syndrome with oro-facial and skeletal symptoms. *European Journal of Medical Genetics* 60(8)

Ahmed, H. et al. 2017. Genetic Overview of Syndactyly and Polydactyly. *Plastic and Reconstructive Surgery - Global Open* 5(11), pp. 1–8.

Al-Ghamdi, M.A. et al. 2020. A classification system for split-hand/ foot malformation (SHFM): A proposal based on 3 pedigrees with WNT10B mutations. *European Journal of Medical Genetics* 63(3), p. 103738.

Al-Qattan, M.M. et al. 2009. Embryology of the upper limb. *The Journal of hand surgery* 34(7), pp. 1340–1350.

Al-Qattan, M.M. 2014. Formation of normal interdigital web spaces in the hand revisited: Implications for the pathogenesis of syndactyly in humans and experimental animals. *Journal of Hand Surgery: European Volume* 39(5), pp. 491–498.

Al-Qattan, M.M. 2019. A Review of the Genetics and Pathogenesis of Syndactyly in Humans and Experimental Animals: A 3-Step Pathway of Pathogenesis. *BioMed Research International* 2019

Al-Qattan, M.M. and Alkuraya, F.S. 2019. Cenani–Lenz syndrome and other related syndactyly disorders due to variants in LRP4, GREM1/FMN1, and APC: Insight into the pathogenesis and the relationship to polyposis through the WNT and BMP antagonistic pathways. *American Journal of Medical Genetics, Part A* 179(2), pp. 266–279.

Al-Zahrāwī, Ḫalaf ibn al-ʿAbbās et al. 1973. *Albucasis on surgery and instruments: a definitive edition of the Arabic text with English translation and commentary*. Wellcome Institute of the History of Medicine.

Asaad, M. et al. 2019. Albucasis: A Pioneer Plastic Surgeon. *Annals of plastic surgery* 83(6), pp. 611–617.

Bacchelli, C. et al. 2001. Cenani-Lenz syndrome with renal hypoplasia is not linked to FORMIN or GREMLIN. *Clinical Genetics* 59(3), pp. 203–205.

Ball, K.F. et al. 2021. Embryology and Classification of Congenital Upper Limb Anomalies. *Congenital Anomalies of the Upper Extremity: Etiology and Management* , pp. 3–35.

Baron, R. and Kneissel, M. 2013. WNT signaling in bone homeostasis and disease: from human mutations to treatments. *Nature Medicine* 19(2), pp. 179–192.

Barrow, J.R. et al. 2003. Ectodermal Wnt3/β-catenin signaling is required for the establishment and maintenance of the apical ectodermal ridge. *Genes & development* 17(3), pp. 394–409.

Bell, J. 1953. *On syndactyly and its association with polydactyly*. Cambridge University Press.

Bosse, K. et al. 2000. Localization of a gene for syndactyly type 1 to chromosome 2q34-q36. *American journal of human genetics* 67(2), pp. 492–497.

Bukowska-Olech, E. et al. 2020. A novel biallelic splice-site variant in the LRP4 gene causes sclerosteosis 2. *Birth Defects Research* 112(9), pp. 652–659.

Bullock, W.A. et al. 2019. Lrp4 Mediates Bone Homeostasis and Mechanotransduction through Interaction with Sclerostin In Vivo. *iScience* 20, pp. 205–215.

Carballo, G.B. et al. 2018. A highlight on Sonic hedgehog pathway. *Cell Communication and Signaling* 16(1), pp. 1–15.

Cenani, A. and Lenz, W. 1967. Totale Syndaktylie und totale radioulnare Synostose bei zwei Brüdern - Ein Beitrag zur Genetik der Syndaktylien. *Zeitschrift für Kinderheilkunde* 101(3), pp. 181–190.

Choi, H.Y. et al. 2009. Lrp4, a novel receptor for dickkopf 1 and sclerostin, is expressed by osteoblasts and regulates bone growth and turnover In Vivo. *PLoS ONE* 4(11)

Clevers, H. 2006. Wnt/β-Catenin Signaling in Development and Disease. *Cell* 127(3), pp. 469–480.

Dai, L. et al. 2014. Mutations in the homeodomain of HOXD13 cause syndactyly type 1-c in two Chinese families. *PLoS ONE* 9(5)

Debeer, P. et al. 2002. The fibulin-1 gene (FBLN1) is disrupted in a t(12;22) associated with a complex type of synpolydactyly. *Journal of medical genetics* 39(2), pp. 98–104.

Delgado, I. and Torres, M. 2017. Coordination of limb development by crosstalk among axial patterning pathways. *Developmental Biology* 429(2), pp. 382–386.

Deng, H. et al. 2017. Identification of a missense HOXD13 mutation in a Chinese family with

syndactyly type I-c using exome sequencing. *Molecular Medicine Reports* 16(1), pp. 473–477.

Díaz-Hernández, M.E. et al. 2014. Molecular control of interdigital cell death and cell differentiation by retinoic acid during digit development. *Journal of Developmental Biology* 2(2), pp. 138–157.

Dimitrov, B.I. et al. 2010. Genomic rearrangements of the GREM1-FMN1 locus cause oligosyndactyly, radio-ulnar synostosis, hearing loss, renal defects syndrome and Cenanie-Lenz-like non-syndromic oligosyndactyly. *Journal of Medical Genetics* 47(8), pp. 569–574.

Drögemüller, C. et al. 2007. Congenital syndactyly in cattle: Four novel mutations in the low density lipoprotein receptor-related protein 4 gene (LRP4). *BMC Genetics* 8, pp. 1–12.

Duchesne, A. et al. 2006. Identification of a doublet missense substitution in the bovine LRP4 gene as a candidate causal mutation for syndactyly in Holstein cattle. *Genomics* 88(5), pp. 610–621.

Foucher, G. et al. 2001. Metacarpal synostosis: a simple classification and a new treatment technique. *Plastic and reconstructive surgery* 108(5), pp. 1224–1225.

Goldstein, D.J. et al. 1994. Familial Crossed Poly sy ndac t yly. 223, pp. 215–223.

Harpf, C. et al. 2005. A variant of Cenani-Lenz syndactyly (CLS): Review of the literature and attempt of classification. *British Journal of Plastic Surgery* 58(2), pp. 251–257.

Hill, R.E. and Lettice, L.A. 2016. 15 - Limb Development. In: Baldock, R. et al. eds. *Kaufman's Atlas of Mouse Development Supplement*. Boston: Academic Press, pp. 193–205.

Holstein, T.W. 2012. The evolution of the wnt pathway. *Cold Spring Harbor Perspectives in*

Biology 4(7), pp. 1–17.

Huybrechts, Y. et al. 2020. WNT Signaling and Bone: Lessons From Skeletal Dysplasias and Disorders. *Frontiers in Endocrinology* 11(April)

Jamsheer, A. et al. 2013. Whole exome sequencing identifies FGF16 nonsense mutations as the cause of X-linked recessive metacarpal 4/5 fusion. *Journal of medical genetics* 50(9), pp. 579–584.

Jarbhou, H. et al. 2008. Cenani-Lenz syndactyly with facial dysmorphism, hypothyroidism, and renal hypoplasia: A case report. *Clinical Dysmorphology* 17(4), pp. 269–270.

Johnson, E.B. et al. 2005. Abnormal development of the apical ectodermal ridge and polysyndactyly in Megf7-deficient mice. *Human Molecular Genetics* 14(22), pp. 3523–3538.

Jordan, D. et al. 2012. The Epidemiology, Genetics and Future Management of Syndactyly. *The Open Orthopaedics Journal* 6(1), pp. 14–27.

Kantaputra, P.N. et al. 2010. A novel homozygous Arg222Trp missense mutation in WNT7A in two sisters with severe Al-Awadi/Raas-Rothschild/Schinzel phocomelia syndrome. *American Journal of Medical Genetics, Part A* 152(11), pp. 2832–2837.

Kariminejad, A. et al. 2013. Severe Cenani-Lenz syndrome caused by loss of LRP4 function. *American Journal of Medical Genetics, Part A* 161(6), pp. 1475–1479.

Karner, C.M. et al. 2010. Lrp4 regulates initiation of ureteric budding and is crucial for kidney formation - a mouse model for cenani-lenz syndrome. *PLoS ONE* 5(4)

Kataoka, K. et al. 2018. Bhlha9 regulates apical ectodermal ridge formation during limb

development. *Journal of bone and mineral metabolism* 36(1), pp. 64–72.

Khan, T.N. et al. 2013. Cenani-Lenz syndrome restricted to limb and kidney anomalies associated with a novel LRP4 missense mutation. *European Journal of Medical Genetics* 56(7), pp. 371–374.

Lan, L. et al. 2019. Roles of Wnt7a in embryo development, tissue homeostasis, and human diseases. *Journal of Cellular Biochemistry* 120(11), pp. 18588–18598.

Leonard Goldner, J. 1975. Congenital Deformities of the Hand and Forearm. *Physical Therapy* 55(11), p. 1290.

Leupin, O. et al. 2011. Bone overgrowth-associated mutations in the LRP4 gene impair sclerostin facilitator function. *Journal of Biological Chemistry* 286(22), pp. 19489–19500.

Li, Y. et al. 2010. LRP4 Mutations Alter Wnt/β-Catenin Signaling and Cause Limb and Kidney Malformations in Cenani-Lenz Syndrome. *American Journal of Human Genetics* 86(5), pp. 696–706.

Lindy, A.S. et al. 2014. Truncating mutations in LRP4 lead to a prenatal lethal form of Cenani-Lenz syndrome. *American Journal of Medical Genetics, Part A* 164(9), pp. 2391–2397.

Logan, C.Y. and Nusse, R. 2004. The Wnt signaling pathway in development and disease. *Annual Review of Cell and Developmental Biology* 20, pp. 781–810.

Luo, J. et al. 2009. [A case-control study on genetic and environmental factors regarding polydactyly and syndactyly]. *Zhonghua liu xing bing xue za zhi = Zhonghua liuxingbingxue zazhi* 30(9), pp. 903–906.

Maeda, K. et al. 2012. Wnt5a-Ror2 signaling between osteoblast-lineage cells and osteoclast precursors enhances osteoclastogenesis. *Nature Medicine* 18(3), pp. 405–412.

Maeda, K. et al. 2019. The regulation of bone metabolism and disorders by wnt signaling. *International Journal of Molecular Sciences* 20(22), p. 5525.

Malik, S. et al. 2005a. Autosomal recessive mesoaxial synostotic syndactyly with phalangeal reduction maps to chromosome 17p13.3. *American journal of medical genetics. Part A* 134(4), pp. 404–408.

Malik, S. et al. 2005b. Evidence for clinical and genetic heterogeneity of syndactyly type I: the phenotype of second and third toe syndactyly maps to chromosome 3p21.31. *European Journal of Human Genetics* 13(12), pp. 1268–1274.

Malik, S. et al. 2006. Genetic heterogeneity of synpolydactyly: A novel locus SPD3 maps to chromosome 14q11.2-q12. *Clinical Genetics* 69(6), pp. 518–524.

Malik, S. 2012. Syndactyly: Phenotypes, genetics and current classification. *European Journal of Human Genetics* 20(8), pp. 817–824.

Man, L.X. and Chang, B. 2006. Maternal cigarette smoking during pregnancy increases the risk of having a child with a congenital digital anomaly. *Plastic and Reconstructive Surgery* 117(1), pp. 301–308.

Maupin, K.A. et al. 2013. A Comprehensive Overview of Skeletal Phenotypes Associated with Alterations in Wnt/β-catenin Signaling in Humans and Mice. *Bone Research* 1(1), pp. 27–71.

May, P. et al. 2007. The LDL receptor-related protein (LRP) family: An old family of proteins

with new physiological functions. *Annals of Medicine* 39(3), pp. 219–228.

Monroe, D.G. et al. 2012. Update on Wnt signaling in bone cell biology and bone disease. *Gene* 492(1), pp. 1–18.

Montero, J.A. et al. 2020. Cell death in the developing vertebrate limb: A locally regulated mechanism contributing to musculoskeletal tissue morphogenesis and differentiation. *Developmental Dynamics* (June), pp. 1–12.

Muragaki, Y. et al. 1996. Altered growth and branching patterns in synpolydactyly caused by mutations in HOXD13. *Science (New York, N.Y.)* 272(5261), pp. 548–551.

Nakayama, M. et al. 1998. Identification of high-molecular-weight proteins with multiple EGF-like motifs by motif-trap screening. *Genomics* 51(1), pp. 27–34.

Ng, J.K. et al. 2002. The limb gene Tbx5 promotes limb initiation by interacting with Wnt2b adn Fgf10. *Development* 129(22), pp. 5161–5170.

Ng, L.F. et al. 2019. WNT Signaling in Disease. *Cells* 8(8), pp. 1–31.

Niemann, S. et al. 2004. Homozygous WNT3 Mutation Causes Tetra-Amelia in a Large Consanguineous Family. *American Journal of Human Genetics* 74(3), pp. 558–563.

Nusse, R. et al. 1991. A new nomenclature for int-1 and related genes: The Wnt gene family. *Cell* 64(2), p. 231.

Nusse, R. and Clevers, H. 2017. Wnt/β-Catenin Signaling, Disease, and Emerging Therapeutic Modalities. *Cell* 169(6), pp. 985–999.

Nusse, R. and Varmus, H.E. 1982. Many tumors induced by the mouse mammary tumor virus

contain a provirus integrated in the same region of the host genome. *Cell* 31(1), pp. 99–109.

Nüsslein-volhard, C. and Wieschaus, E. 1980. Mutations affecting segment number and polarity in drosophila. *Nature* 287(5785), pp. 795–801.

Ohazama, A. et al. 2010. Lrp4: A novel modulator of extracellular signaling in craniofacial organogenesis. *American Journal of Medical Genetics, Part A* 152 A(12), pp. 2974–2983.

Patel, N. et al. 2015. A novel APC mutation defines a second locus for cenani-lenz syndrome. *Journal of Medical Genetics* 52(5), pp. 317–321.

Paznekas, W.A. et al. 2003. Connexin 43 (GJA1) mutations cause the pleiotropic phenotype of oculodentodigital dysplasia. *American journal of human genetics* 72(2), pp. 408–418.

Petit, F. et al. 2017. Limb development: A paradigm of gene regulation. *Nature Reviews Genetics* 18(4), pp. 245–258.

Rayan, G.M. and Upton III, J. 2014. Syndactyly. In: *Congenital Hand Anomalies and Associated Syndromes*. Berlin, Heidelberg: Springer Berlin Heidelberg, pp. 367–393.

Rijsewijk, F. et al. 1987. The Drosophila homology of the mouse mammary oncogene int-1 is identical to the segment polarity gene wingless. *Cell* 50(4), pp. 649–657.

Schneider, W.J. and Nimpf, J. 2003. LDL receptor relatives at the crossroad of endocytosis and signaling. *Cellular and Molecular Life Sciences* 60(5), pp. 892–903.

Seven, M. et al. 2000. A variant of Cenani-Lenz type syndactyly. *Genetic counseling (Geneva, Switzerland)* 11(1), p. 41—47.

Shen, C. et al. 2015. LRP4 in neuromuscular junction and bone development and diseases. *Bone*

80, pp. 101–108.

Steel, E. et al. 2020. Cenani-Lenz syndactyly in siblings with a novel homozygous LRP4 mutation and recurrent hypoglycaemia. *Clinical Dysmorphology* 29(2), pp. 73–80.

Sukenik Halevy, R. et al. 2018. Mutations in the fourth β-propeller domain of LRP4 are associated with isolated syndactyly with fusion of the third and fourth fingers. *Human Mutation* 39(6), pp. 811–815.

Swanson, A.B. 1976. A classification for congenital limb malformations. *Journal of Hand Surgery* 1(1), pp. 8–22.

Temtamy, S.A. et al. 2003. Mild facial dysmorphism and quasidominant inheritance in Cenani-Lenz syndrome. *Clinical Dysmorphology* 12(2), pp. 77–83.

Temtamy, S.A. and McKusick, V.A. 1978. The genetics of hand malformations. *Birth defects original article series* 14(3), pp. i–xviii, 1–619.

Teufel, S. and Hartmann, C. 2019. *Wnt-signaling in skeletal development*. 1st ed. Elsevier Inc.

Tian, J. et al. 2019. Deficiency of lrp4 in zebrafish and human LRP4 mutation induce aberrant activation of Jagged–Notch signaling in fin and limb development. *Cellular and Molecular Life Sciences* 76(1), pp. 163–178.

Tickle, C. and Towers, M. 2017. Sonic hedgehog signaling in limb development. *Frontiers in Cell and Developmental Biology* 5(FEB), pp. 1–19.

Tripolszki, K. et al. 2016. Somatic mosaicism of the PIK3CA gene identified in a Hungarian girl with macrodactyly and syndactyly. *European Journal of Medical Genetics* 59(4), pp. 223–226.

Turner, N. and Grose, R. 2010. Fibroblast growth factor signalling: From development to cancer. *Nature Reviews Cancer* 10(2), pp. 116–129.

Umair, M. et al. 2018. Syndactyly genes and classification: a mini review. *Journal of Biochemical and Clinical Genetics* 1(December 2017), pp. 10–18.

Verheyden, J.M. and Sun, X. 2008. An Fgf/Gremlin inhibitory feedback loop triggers termination of limb bud outgrowth. *Nature* 454(7204), pp. 638–641.

Waterhouse, A.M. et al. 2009. Jalview Version 2—a multiple sequence alignment editor and analysis workbench. *Bioinformatics* 25(9), pp. 1189–1191.

Weatherbee, S.D. et al. 2006. LDL-receptor-related protein 4 is crucial for formation of the neuromuscular junction. *Development* 133(24), pp. 4993–5000.

White, J.J. et al. 2018. WNT Signaling Perturbations Underlie the Genetic Heterogeneity of Robinow Syndrome. *American Journal of Human Genetics* 102(1), pp. 27–43.

Wiese, K.E. et al. 2018. Wnt signalling: Conquering complexity. *Development (Cambridge)* 145(12), pp. 1–9.

Winter, R.M. and Tickle, C. 1993. Syndactylies and polydactylies: embryological overview and suggested classification. *European journal of human genetics : EJHG* 1(1), pp. 96–104.

Witte, F. et al. 2009. Comprehensive expression analysis of all Wnt genes and their major secreted antagonists during mouse limb development and cartilage differentiation. *Gene Expression Patterns* 9(4), pp. 215–223.

Woods, C.G. et al. 2006. Mutations in WNT7A cause a range of limb malformations, including

fuhrmann syndrome and Al-Awadi/Raas-Rothschild/Schinzel phocomelia syndrome. *American Journal of Human Genetics* 79(2), pp. 402–408.

Wu, L. et al. 2009. A ZRS duplication causes syndactyly type IV with tibial hypoplasia. *American journal of medical genetics. Part A* 149A(4), pp. 816–818.

Yamaguchi, Y.L. et al. 2006. Expression of low density lipoprotein receptor-related protein 4 (Lrp4) gene in the mouse germ cells. *Gene Expression Patterns* 6(6), pp. 607–612.

Yang, Y. 2003. Wnts and wing: Wnt signaling in vertebrate limb development and musculoskeletal morphogenesis. *Birth Defects Research Part C: Embryo Today: Reviews* 69(4), pp. 305–317.

Zhao, X. et al. 2007. Mutations in HOXD13 underlie syndactyly type V and a novel brachydactyly-syndactyly syndrome. *American journal of human genetics* 80(2), pp. 361–371.

Zhao, X. et al. 2010. Retinoic acid controls expression of tissue remodeling genes Hmgn1 and Fgf18 at the digit-interdigit junction. *Developmental dynamics : an official publication of the American Association of Anatomists* 239(2), pp. 665–671.

CHAPTER 10

Appendix I

Primer Sequences

Table 10. 1: Primers sequences used for Sanger sequencing

Primer Name	Sequence
LRP4_C1017R	**Forward: 5'**-GCAGCAGGACTCATGGTTTC-**3'** **Reverse: 5'**-GAGCGCATCTATTGGACTGAC-**3'**
LRP4_ T461P	**Forward: 5'**-GAGTACCTGGCCTTCCTCC-**3'** **Reverse: 5'**-GAGTGGGAGGACGACAGAAG-**3'**